LASER
& PHOTONICS
REVIEWS

Laser Photonics Rev. **9,** No. 3, 309–329 (2015) / **DOI** 10.1002/lpor.201500006

Abstract Subwavelength features in conjunction with light-guiding structures have gained significant interest in recent decades due to their wide range of applications to particle and atom trapping. Lately, the focus of particle trapping has shifted from the microscale to the nanoscale. This few orders of magnitude change is driven, in part, by the needs of life scientists who wish to better manipulate smaller biological samples. Devices with subwavelength features are excellent platforms for shaping local electric fields for this purpose. A major factor that inhibits the manipulation of submicrometer particles is the diffraction-limited spot size of free-space laser beams. As a result, technologies that can circumvent this limit are highly desirable. This review covers some of the more significant advances in the field, from the earliest attempts at trapping using focused Gaussian beams, to more sophisticated hybrid plasmonic/metamaterial structures. In particular, examples of emerging optical trapping configurations are presented.

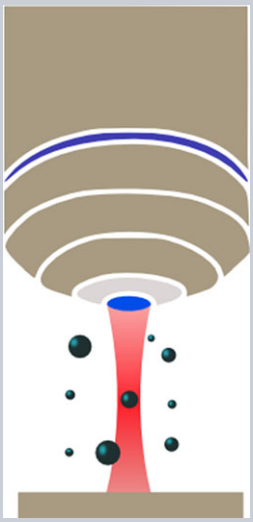

REVIEW
ARTICLE

Optical trapping and manipulation of micrometer and submicrometer particles

Mark Daly, Marios Sergides, and Síle Nic Chormaic*

1. Introduction

The idea that particles could be influenced by the radiation pressure from light has existed as a concept for a very long time; almost 400 years ago Johannes Kepler published a treatise entitled "*De cometis libelli tres*" [1], wherein he proposed that solar rays were the cause of the deflection of a comet's tail. However, it was not until much later, when Maxwell formalized his theory of electromagnetism, that this force could be quantified. In 1906, John Henry Poynting, in relation to the force induced by radiation pressure, stated that "*even here, so minute is the force that it only need be taken into account with minute bodies*" [2]. The next major milestone on the road to harnessing radiation pressure came with the discovery and invention of the laser in 1960 [3].

Just over two decades after the first operational laser was created, Ashkin et al. published their seminal paper in which they proposed and demonstrated how a laser could be used to trap and manipulate micrometer- and submicrometer-sized dielectric particles by considering the total conservation of momentum in a light–particle system [4]. The initial design for the "*optical tweezers*", as the design based on Ashkin's seminal work came to be known, required very few optical components, with the laser source being the most costly. While Ashkin pioneered the work [5], other research groups quickly began to improve upon the design to make it more versatile. Modern optical tweezers allow for a high degree of control over several trapping parameters, such as particle location and trap strength. This has been achieved by including components such as acousto-optical deflectors, servo-controlled mirror arrays, etc. to create multiple trapping sites and/or to provide control over the particle's motion in the 2D focal plane of the optical tweezers. Optical tweezers are capable of performing high-resolution measurements when it comes to sensing small displacements of the trapped objects. This property has made the technique of interest in the life sciences where, typically, such small measurements of displacement, or force, were previously very difficult to examine.

In more recent years, the field of optical trapping has benefitted greatly from advances in other optics-related areas. To overcome limitations imposed by the diffraction limit of free-space laser beams, the research direction of many optical manipulation groups has shifted to devices that exploit optical near-fields. Optical near-fields, unlike far-fields, can create subdiffraction-limited spot sizes. Near-field devices range from the superresolution lens as described by Pendry [6] to the use of surface plasmons [7, 8] created by the coherent oscillation of electrons near

Light-Matter Interactions Unit, OIST Graduate University, Onna, Okinawa, 904-0495, Japan
*Corresponding author: e-mail: sile.nicchormaic@oist.jp

the boundary of a metal–dielectric system. Both of these designs are capable of creating electric field 'hotspots' that can greatly enhance the field strength locally.

This review seeks to outline the current state of the field while focusing mainly on methods that can be employed to shift optical trapping into the nanometer regime through the use of methods and techniques that are not overly complex in design. The scope of the field of optical trapping makes a complete review an almost impossible task. This paper touches on many aspects of optical trapping, but for extensive reviews of the biological applications of optical tweezers, or more indepth discussions about how optical tweezers can be improved by algorithms or diffractive elements, the reader's attention is drawn to other reviews [9–11].

Section 2 mentions a few of the important applications that have stemmed from the field of optical trapping in order to provide some motivation for the work as a whole. Section 3 outlines the fundamental theory behind optical trapping along with details about where more rigorous calculations of the trapping forces can be found. Sections 4 through 6 review a subset of the many types of traps used in optical manipulation today, with the order of the sections somewhat governed by the decreasing size of the particles that can be trapped.

2. Applications

The field of optical trapping, as with many scientific fields, is motivated by the potential applications that can stem from it. The high degree of control and precision with which one can trap and localize particles using optical tweezers, or other similar trapping systems based on optical forces, is impressive in and of itself, but it is the ability to then apply these techniques experimentally with incredible resolution that is of interest to scientists, especially those in the life sciences.

One of the most common applications of optical tweezers is the strong confinement and manipulation of small objects. For example, Waleed et al. used optical tweezers to spatially localize plasmid-coated microparticles that were then optically inserted into MCF-7 cells. The cells were optically perforated using a femtosecond laser to guarantee transfection [12]. In this work the versatility of the optical tweezers is shown since, not only were the optical tweezers used to manipulate the particle's position, but they were also used to experimentally determine the focal length of various laser sources.

Other work has been done using optical tweezers to measure exceptionally minute position changes with high resolution. Examples include measuring the step sizes of kinesin proteins along microtubules [13], the distance between adjacent basepairs via determination of the step sizes of DNA polymerase [14], and, more recently, unwinding–rewinding dynamics in P-fimbriae [15]. Some of these applications will be discussed in more detail in Section 4.2.

Application of force to trapped particles can also be achieved using optical tweezers system, and this has been exploited to analyse biological systems. By incorporating optical tweezers with Förster resolved energy transfer (FRET) [16], conformational dynamics of Holliday junctions and the folding dynamics of DNA hairpins have been measured. Integrating optical tweezers with other spectroscopic and microscopic techniques is a vital step in the furthering of their applications in the life sciences. This has led to the integration of optical tweezers with techniques such as Raman spectroscopy (see Section 4.3) and stimulated emission depletion (STED) fluorescence microscopy [17–19]. All of these modifications have served to further increase the effectiveness of optical tweezing techniques in many fields.

Moving from manipulating 'large', i.e. micrometer-sized, particles to smaller nanoscale particles opens up a vast array of applications. The previous examples, which certainly involved the investigation of nanoscale objects such as DNA, were only able to do so via the use of micrometer-sized spheres. A lot of research in the field is, therefore, focused on overcoming this size limitation. Eventually, we can expect that trapping small particles, such as bacteria and viruses, will become routine. This would be an excellent achievement for the nanobiology world [20] and some progress in this direction has already been made. For example, influenza viruses, of about 100 nm size, have been individually manipulated using optical forces alone [21]. Within this review we aim to discuss some of the progress made in these applications, commencing with the introduction of the more well-established techniques in the field.

3. Optical trapping regimes

The first applications of light to trap particles utilized a technique that came to be known as optical tweezing. By employing a tightly focused Gaussian beam, particles can be trapped near the focus due to the gradient force induced by the momentum exchange of photons with the dielectric particles. Ashkin proposed the application of focused Gaussian beams for both particle [5] and atom trapping [22] using radiation pressure, albeit almost a decade apart. The description of how a particle behaves in a light field can be described using different models that depend on the particle's size in relation to the wavelength of the light used for trapping. For example, if the particle is large in comparison to the wavelength, a ray-optics approach can be used. Since this review focuses on the transition between the micro- and nanoworlds of optical trapping, the details of the ray-optics approach will not be discussed. However, the simple ray-optics explanation does provide a somewhat intuitive model for how trapping occurs, and should not be discarded as an invalid approach to describing the optical forces on particles.

3.1. Rayleigh regime

For particles with sizes equal to, or smaller than, the wavelength of light, an electromagnetic model is required to adequately represent the forces at play in a particle–light system. This solution can range from a more complete theory, which uses the Mie solutions to scattering problems involving spherical or elliptical objects, to a simpler case when the particle size is much smaller than the wavelength of the trapping light and is made from a linear, isotropic material. This allows for the use of the dipole approximation in the calculations. The polarizability of a particle in this case gives rise to a dipole moment, $\vec{p}$

$$\vec{p} = \alpha \vec{\mathrm{E}}, \tag{1}$$

where α is the particle's polarization and $\vec{E}$is the electric field. The electrostatic potential generated by a dipole in an electric field is related to this polarizability via $\vec{U} = -\vec{p}.\vec{E}$. Hence, the force, which is the negative gradient of the potential, can be determined

$$\vec{F} = -\nabla U = -\nabla\left(\vec{p}.\vec{E}\right) = -\alpha\nabla\vec{E}^{2}. \tag{2}$$

Because of this polarization dependence, metallic nanoparticles, which, over wavelengths of interest in particle trapping have a much higher polarizability, are often used as targets for trapping at the nanoscale since they require the use of lower optical powers compared to silica or polystyrene particles of the same size. Taking the time average of the field into account, and using the Clausius–Mossotti relationship for a spherical dielectric particle, the so-called gradient force a particle feels is finally given as

$$\vec{F}_{grad} = -\frac{2\pi n_0 r^3}{c}\left(\frac{m^2-1}{m^2+2}\right)\nabla I(\vec{r}), \tag{3}$$

where r is the particle's radius, c is the speed of light, n_0 is the refractive index of the medium, m is the dielectric contrast, i.e. the ratio of the particle's index to the medium's index, and $I(\vec{r})$ is the time-averaged intensity as a function of position, $\vec{r}$. The dielectric contrast plays a role in the trapping strength of optical tweezers, but more interestingly, changing the value of this property can cause the sign of the force to be reversed. If particles of a lower index than their surrounding medium are used, i.e. $m < 1$, the sign of Eq. (3) is seen to change. The origin of the term "*gradient force*" should now be evident from Eq. (3); it is a force that is linearly dependent on the gradient of the intensity and tends to attract particles to regions of higher, or lower, intensity pending the value of the dielectric contrast.

Stable trapping occurs when the net force on a particle is zero and any small displacements from this stable position result in an optical force that resists the motion of the particle away from this position. Typically, traps with a potential depth greater than the thermal limit, i.e. a few k_bT, are required for stable trapping, where k_b is the Boltzmann constant and T is the particle's temperature. A potential depth in the region of $10k_bT$ is often used as a standard value for stable traps.

To complete the discussion on optical forces, one must also include the scattering force felt by a particle that is being bombarded by a flux of photons of wavenumber k. Under the Rayleigh approximation, along with the Clausius–Mossotti relationship, this is given as

$$\vec{F}_{scatt} = \frac{8\pi n_0 k^4 r^6}{3c}\left(\frac{m^2-1}{m^2+2}\right)^2 I(\vec{r})\vec{z}. \tag{4}$$

If the problem is approached using a more rigorous calculation involving the Maxwell stress tensor or Lorentz force, a third force, known as the polarization gradient force, arises out of the calculations; this force is typically not present in trapping systems, but its existence should be noted [23].

3.2. Mie solutions and discrete dipole approximation

For particles of intermediate sizes, between that of the ray optics and Rayleigh regimes, one can apply the Mie solutions [24, 25]. These solutions are the complete solutions to the Helmholtz equation that take the form of an infinite series. The Mie solutions are very important in this size regime. In the Rayleigh regime the force scales as the cube of the particle's radius and this can be shown to be incorrect for larger particles in the ray-optics regime. The Mie solutions help to bridge this gap between the two regimes, while also introducing some new phenomena which would otherwise be unnoticed in the theory. In a paper by Stilgoe et al. [26] a detailed calculation of the trapping forces on particles of varying radii and refractive indices using different numerical apertures is described. A phenomenon known as a Mie resonance occurs in intermediate-sized particles, and this is more prominent in particles with a higher refractive index contrast between them and the medium. The presence of Mie resonances strongly changes the trap strength of optical tweezers, as can be seen from Fig. 1 [26], and should be taken into account when developing tweezers to work at such particle sizes in order to maximize its effectiveness. As can be seen in Fig. 1b, the interference effects can cause the trap strength to oscillate between trapping and nontrapping regions as the particle size is changed, an effect that is absent in the Rayleigh regime.

If the high accuracy of Mie solutions is not required, but work is being done at or near the boundary between the Rayleigh and Mie regimes, the dipole can instead be approximated as a discrete sum of dipoles to reduce the errors arising from the single-dipole approximation.

3.3. Other forces

To fully model an optical manipulation system other forces must be considered, such as the Stokes' drag of a particle and the force due to the random Brownian motion. A

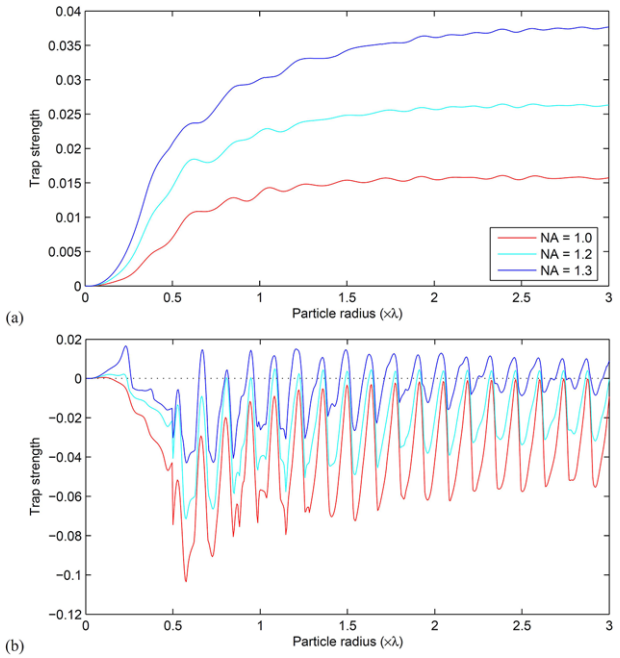

Figure 1 Dependence of the trapping force for (a) polystyrene and (b) diamond particles for a fixed numerical aperture, and particle radii varying between 0 to 3 λ. Note the pronounced interference effects present in the higher refractive index, diamond particles. (Reproduced with permission.[26] 2008, Optics Express).

further discussion of Brownian motion can be found in Section 4.1. The Stokes' drag present in a system can be quite complicated to determine due to the influence of nearby surfaces. For optical tweezers, Faxen's law [27, 28] is often used to include the influence of the nearby planar surfaces, such as coverslips, in an experiment. Often these effects can be solved for experimentally by modeling the system as a damped harmonic system and calibrating accordingly.

4. Optical tweezers with free-space laser beams

Modular optical tweezers using free-space Gaussian beams are highly versatile tools that have high trap stiffness when dealing with micrometer- and, to some degree, submicrometer-sized objects. This is a necessary requirement for precise trapping. They also have incredible resolution with respect to position or force measurements on trapped objects. It is this resolution that makes optical tweezers invaluable in the life sciences. Applying this type of optical tweezers to the problem of trapping dielectric particles does have two drawbacks when it comes to trapping smaller particles. The first arises from the diffraction limit, which limits the waist size of a Gaussian beam refracted through a lens. The second drawback is, admittedly, also a side-effect of the diffraction limit; particles of increasingly smaller size require larger gradient forces to trap them. Photons directly exchange energy with particles via scattering; this force is typically called the scattering force and on average acts in the direction of beam propagation. In the Rayleigh regime, the ratio of the gradient force to the scattering force yields an inverse cube dependence on radius. Taking this value at the position of maximal axial intensity gradient yields [4]

$$R = \frac{F_{grad}}{F_{scatt}} = \frac{3\sqrt{3}}{64\pi^5}\frac{n}{\left(\frac{m^2-1}{m^2+2}\right)}\frac{\lambda^5}{r^3\omega_0^2} \geq 1, \qquad (5)$$

where ω_0 is the focal spot size. This puts an upper limit on the particle size, since the gradient force must dominate. However, the time needed for a particle to be trapped must also be longer than the diffusion time out of the trap to ensure efficient trapping. Trapping objects in the nanometer regime requires laser powers that can quickly destroy/denature the samples being trapped. Despite this, optical tweezers systems using focused Gaussian beams remain invaluable tools.

4.1. Optical tweezers basics

The term 'optical tweezers' refers to any optical system that is capable of confining a particle in all three dimensions. The most commonly available system involves the use of free space optical beams to provide a gradient force trap in all directions. Recently, commercial, self-calibrating optical tweezers systems have become available, indicating the rise of interest in the field.

Free-space optical tweezers exist in many different varieties due to their high customizability. As mentioned previously, optical tweezers typically use focused Gaussian beams (Fig. 2) combined with some mechanism that can deflect or otherwise steer the light beam in the focal plane of the tweezers. Some examples include galvanometer-mounted mirror arrays to create multiple trapping sites by rapidly moving the trap center around the focal plane [29], holographic optical tweezers that include a spatial light modulator (SLM) to create different trapping patterns, acousto-optic deflectors, and even diffractive or polarizing elements. Each variation of optical tweezers has advantages and disadvantages. For example, SLMs allow for a higher degree of control and customizability, but have typically low response times [11, 30, 31]. Both continuous-wave (CW) or pulsed lasers can be used in optical tweezers [32].

The operation of optical tweezers is typically chosen to be in the near-infrared region, primarily because light of wavelengths greater than 800 nm is poorly absorbed by most living matter and, as one moves further into the far-infrared region, absorption from water molecules becomes an issue [33]. For these reasons, light from an Nd:YAG laser at approximately 1064 nm is commonly used for optical trapping. Optical tweezers are capable of resolving subnanometer motion and measuring pN of force [14].

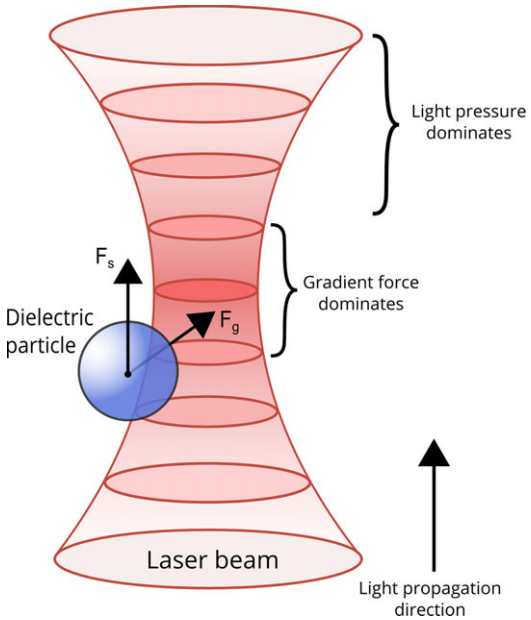

Figure 2 Schematic of a Gaussian beam optical tweezers (red) showing a particle (blue) along with the scattering (F_s) and gradient (F_g) forces that act upon it. The darker shades of red indicate regions of higher intensity.

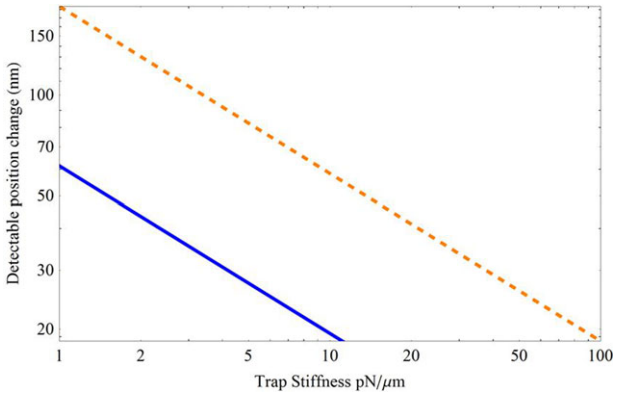

Figure 3 Log-log plot of detectable position change versus trap stiffness at the thermal limit (blue solid line) which corresponds to 68.5% detection efficiency, and three times the thermal limit (orange dashed line) which corresponds to 99.7% detection efficiency.

For optical tweezers in viscous media, the motion of the trapped particle can be well described by an overdamped Langevin model, often termed the "Einstein–Ornstein–Uhlenbeck theory of Brownian motion" [34]. In this overdamped regime, the inertia terms in the Langevin equation become negligible and the power spectrum of the system can be well described. To put it simply, the fundamental operational limit for measurements using optical tweezers, or indeed in any of the systems that will be discussed herein, is due to Brownian noise. This noise is always present and, unlike other measurement-based errors such as laser noise, shot noise, imaging errors, etc., it cannot be circumvented. A particle's motion while trapped in optical tweezers can be described as a harmonic oscillator. Therefore, it is easy to equate the energy of the particle's Brownian motion to the trap's energy using the equipartition theorem, i.e. $\frac{1}{2}k_bT = \frac{1}{2}\kappa\langle\chi^2\rangle$ [35], where k_b is Boltzmann's constant, T is the temperature, κ is the spring constant of the system, and $\langle\chi^2\rangle$ is the particle's mean squared displacement from equilibrium. This can be used to determine the fundamental measurement limit for experiments based on optical tweezers. By defining the square root of the mean squared displacement as $\sqrt{\chi^2} = \sqrt{k_bT/\kappa}$, the minimum detectable limit can be determined, as shown in Fig. 3. To measure the trap stiffness, a simple Lorentzian can be fitted to the power spectrum, but this gives errors of 10–20%. Further studies have shown how to increase the accuracy of such a measurement via modification of the Lorentzian fit [36].

The assumption that one can work at this Brownian noise limit is of course, untrue, as there will always be sources of error that cannot be entirely eradicated. One can, however, work extremely close to this limit. Many attempts have been made over the years to reduce noise and increase trapping times in optical tweezers. These approaches range from the use of laser feedback control algorithms to reducing the average laser power and hence the associated noise, to the use of interferometric techniques to enhance sensitivity [13, 37].

Although not discussed in detail in this review, it is worth mentioning that the problems of noise for optical tweezers in vacuum, such as that associated with optically levitated particles, are different. Earlier, we dealt with an overdamped system, but, in vacuum, the system is underdamped as there is no viscous medium to interact with the trapped particle. Aside from the other effects that this has on optical trapping, it also means that the measurement limit now becomes a problem more strongly related to the laser intensity, or, rather, the photon flux. Recoil energy is directly imparted to the particles via interaction with the photons in the laser beam. This is in many ways similar to the laser cooling of atoms in a magneto-optical trap, where the thermal limit comes not from any interaction with residual gases in the vacuum, but rather from the recoil energy of the laser photons.

An influential application of optical tweezers was performed in 1993 by Svoboda et al. [13]. They concluded that kinesin, a type of motor protein found in eukaryotic cells, moved in 8-nm steps. In this early application of optical tweezers, silica beads were coated with kinesin in such a way as to allow only a single active molecule per bead. These beads were then attached to microtubules along which kinesin can move and measurements of the step size were made using overlapping beams from a Wollaston prism. Phase objects, such as silica beads, placed in the overlapping region caused varying degrees of ellipticity in the recombined beam and this effect was used to determine fine movements of the objects. This extra step was required to achieve the 8-nm resolution reported and helped show the versatility of optical tweezers in biology.

4.2. Dual-beam optical tweezers

Single-beam traps are at a disadvantage when compared with dual- or multiple-beam optical tweezers since only one particle can be steered or guided at any given time. Multiple-beam traps can be created numerous ways, such as the time sharing of a single beam using motorized mirror arrays, or the splitting of a single beam via polarization elements to create two individual trapping potentials. A particle suspended in the optical gradient of a beam is somewhat decoupled from the environment, but measurements generally require that a second object, which is directly coupled to the environment via some physical stage or mount, be used. This second particle is subject to many forms of external noise, such as stage drift that often dominates the noise spectrum.

Dual-beam optical tweezers are systems that, effectively, combine two single-beam optical tweezers. This allows one to simultaneously trap two objects and perform differential detection measurements, thereby improving the attainable spatial resolution [10]. Traps of this form existed as early as 1993, although large improvements in stability were shown only about a decade later. Comparing the 8-nm resolution previously obtained [13] to a more recent measurement using a dual-beam trap, an impressive leap in measurement accuracy can be seen, though admittedly this jump was not entirely due to the dual-beam configuration itself.

In 2005, base-pair stepping by RNA polymerase was measured and step sizes of 3.7 Å were distinguishable [14]. This level of high resolution was made possible both through the use of a dual beam tweezers, as well as isolating the system from external air currents via the use of a helium-filled enclosure. The inset of Fig. 4b indicates the drastic drop in noise due to the helium enclosure. By immobilizing both sides of the RNA polymerase with separate optical tweezers, the noise induced by the motion of the stage was effectively removed. The improved signal-to-noise ratio of dual-beam traps has been quantified by Moffitt et al. [38]. The system behaves like a three-spring system consisting of two optical tweezers and a DNA strand as the extra spring. Autocorrelations in the motions of two spheres tethered by a DNA strand, as illustrated in Fig. 4a were measured to determine the 3.7 Å step size. This study showed strong agreement between theory and experiment over the study's chosen parameter range.

Optical tweezers are also used to apply forces. One such example is the combination of an optical trap with a three-color FRET process. In a FRET system, the energy transfer is strongly dependent on the distance between donor and acceptor chromophores [39]. The energy-transfer efficiency is given as:

$$E = \frac{1}{1 + \left(\frac{R}{R_0}\right)^{6'}} \tag{6}$$

where R is the distance between the chromophores and R_0 is a characteristic value called the Förster distance. This Förster distance is where the energy, E, drops to 50% of the maximum and typically the values are in the range of 30–60 Å.

The discovery of fluorescent proteins, which have become ubiquitous in the life sciences, allow direct fluorescence measurements to be made by labeling individual molecular components with different color dyes. This is extremely useful in many fields of study where, for example, the mechanism that needs to be studied is inaccessible due to being part of a minute, complex system. This is true for many biomolecular machines with changing internal conformations. Lee and Hong [16] used this hybrid FRET optical-tweezers system to observe the conformational dynamics of a Holliday junction and the folding dynamics of a DNA hairpin (Fig. 5). Holliday junctions are junctions formed by the intersection of DNA strands, while DNA hairpins are common patterns that can be formed by single DNA strands. Holliday junctions have two distinct conformations (known as ISO1 and ISO2) in the absence of mechanical tension. The authors sought to determine if an applied force showed a bias towards either shape. By labeling different sections of the junction with different dyes, the FRET efficiencies between different pairs were calculated as functions of the applied force and, hence, the shape of the junctions could be deduced. Using a similar technique, folding and unfolding dynamics of a DNA hairpin were studied. The conclusion was that hybrid systems, such as the one discussed in the paper, are readily applicable to many nucleic acid systems.

4.3. Non-Gaussian beam shapes

Alternative approaches to optical tweezing make use of non-Gaussian trapping beams [40]. For example, Tatarkova et al. [41] made use of a zeroth-order Bessel beam generated using an axicon grating. By illuminating the axicon with a slightly converging laser beam they were able to produce a so-called 'washboard' potential with a controllable tilt, i.e. a harmonic potential with a superimposed sinusoidal fluctuation, as illustrated in Fig. 6. When the inclination of the washboard potential exceeded a certain value the particles were drawn to the Bessel beam center.

Optical beams can also have two different types of angular momentum – spin angular momentum and orbital angular momentum (OAM) – both of which can be exploited for particle trapping. Spin angular momentum is related to the polarization of light, whereas OAM is related to the topological phase of light, which gives rise to vortex beams where the phase changes as a function of the beam radius, and can even be transferred to plasmon fields as will be discussed in Section 4 [42–44]. Standing-wave traps generated by counterpropagating Bessel beams have been constructed. Cîzmár et al. [45] successfully trapped particles of diameters from 490 nm to 1000 nm using what they termed a "sliding Bessel standing wave". Using this they constructed an 'optical conveyor belt' by controlling

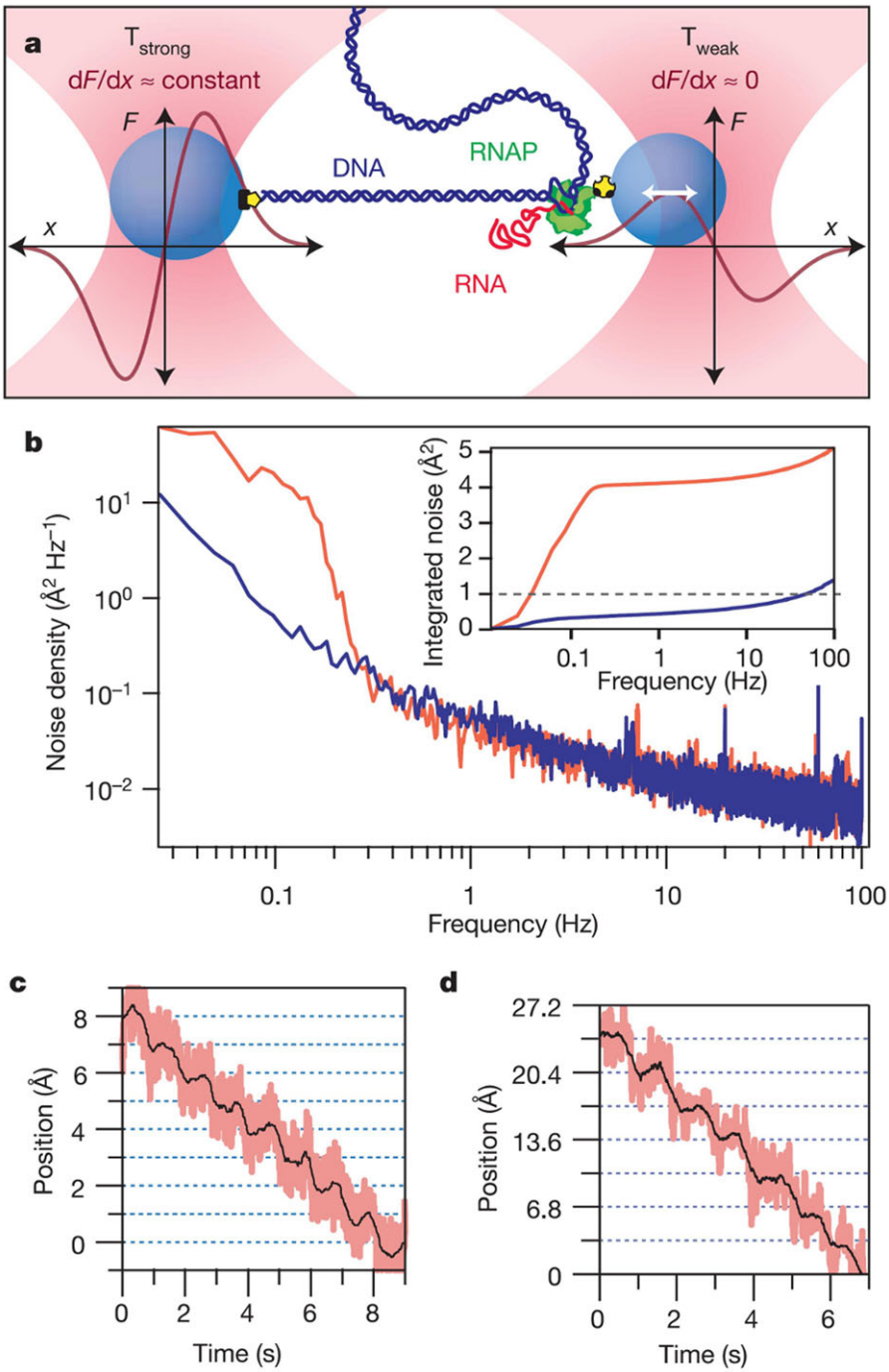

Figure 4 RNA polymerase immobilised using a dual beam optical tweezers and polystyrene beads. T_{strong} and T_{weak} are names given to the traps which refer to them having high and low spring constants respectively. (b) Noise density for helium enclose, blue, and the unenclosed system, red. (c), Steps resolved for a stiffly trapped bead moved in 1 Å increments at 1 Hz. (d) 3.4 Å steps by using a bead-DNA-bead tension of 27 pN then moving T_{strong} in 3.4-A° increments at 1 Hz. (Reproduced with permission.[14] 2005, Nature)

the positions of the nodes and antinodes of the trapping potential generated.

The differences between the two kinds of angular momenta are evident when the effects they have upon particles are considered. Spin angular momentum causes particles to rotate around their axes, whereas OAM can directly impart angular momentum, thereby causing the entire particle to rotate within the field. Furthermore, if the particle is large enough, rotation about an axis is possible with OAM. OAM can be contained within Laguerre–Gaussian (LG) modes, which are frequently used for work in the field. LG beams are particularly useful when fine control of a particle's orientation is required. For example, Dasgupta et al. [18] performed Raman spectroscopy on red blood cells with the help of a Laguerre–Gaussian beam generated from an SLM. The use of Raman spectroscopy techniques combined with optical tweezers has been termed 'Raman tweezers' [19] and is a viable approach that has existed for well over two decades. Optical tweezers have the distinct advantage of being able to make measurements on red blood cells, or

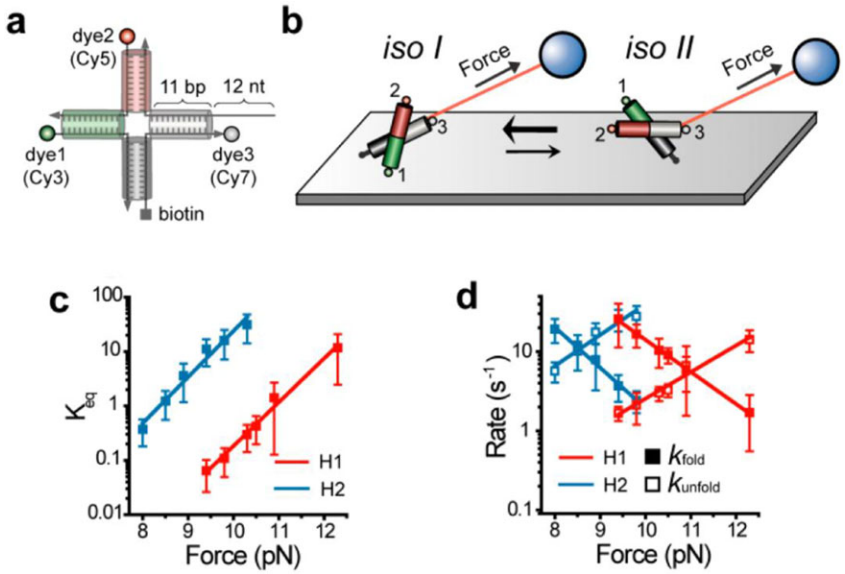

Figure 5 (a) Representative diagram of a Holliday junction. (b) Force is applied to two different conformations of the Holliday junction. (c) The equilibrium constant of the unfolded state (where K_{eq} is the ratio of the unfolded state population to the folded state population) as a function of force, and (d) the rate constants of folding/unfolding reactions as functions of force for H1 (red) and H2 (blue) conformations. (Reproduced with permission.[16] 2013, J. Am. Chem. Soc.)

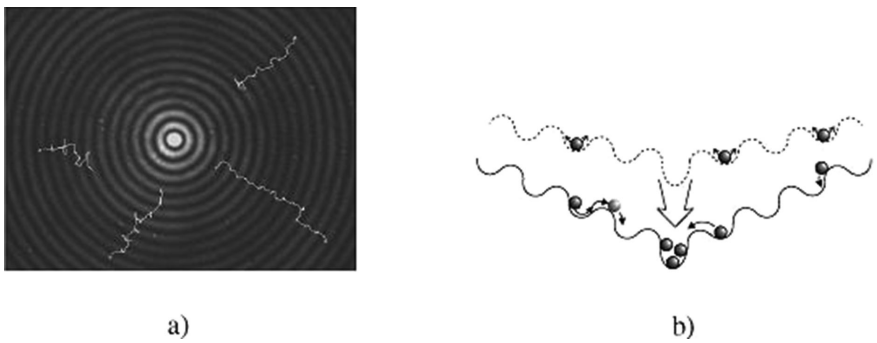

Figure 6 (a) Intensity profile of the zeroth-order Bessel beam produced from an axicon with particle trajectories superimposed upon the image (b) examples of a washboard lattice at two different inclination angles. (Reproduced with permissions.[41] 2003, Phys. Rev. Lett.)

indeed any suitably sized cell, in vitro. Hence, the way a cell behaves during applications of stretching induced stress can be recorded. In the experiment by Dasgupta et al. [18], they showed that LG beams can efficiently trap and control the orientation of blood cells in three dimensions and how this may facilitate polarized Raman spectroscopy of the cells. Larger cells, such as red blood cells, are easier to manipulate with OAM as their bodies can take up a larger portion of the beam allowing for easier rotation.

Certain cells, e.g. E. Coli [46], can be rotated and controlled due to their asymmetric shapes. Spherical particles are, in general, harder to orient accurately. Due to their symmetry, momentum must be imposed via the light's spin or angular momentum. Optical tweezing using cylindrical objects, 1D chains, or birefringent objects has been performed [47]. In 2004, La Porta and Wang [48] published a study that investigated the torque present when birefringent particles were illuminated by an external field. In birefringent materials, the polarization field generated is not aligned with the external electric field, and this produces enough torque to rotate a particle. The authors showed how the position and rotation of a 1-μm quartz particle could be precisely controlled by varying the external field's polarization. Asymmetric objects also rotate in polarization fields

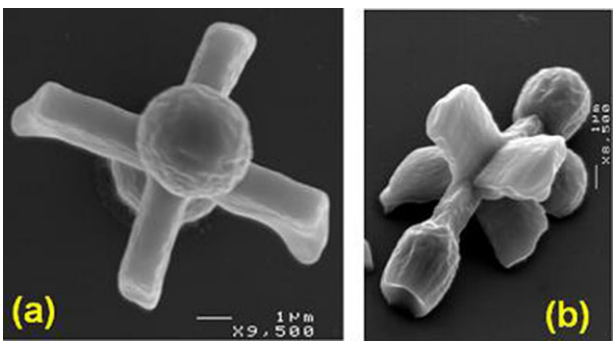

Figure 7 SEM images of a paddle wheel created using two-photon excitation of UV absorbing liquid resins. (Reproduced with permission.[50] 2013, New J. Phys.)

[49]. Asavei et al. [50] microfabricated a paddle wheel, shown in Fig. 7, which could be used in conjunction with a polarized external field to apply controlled fluid flow to specific regions. Many other microfabricated structures have been proposed, and – in some cases – created, to perform specific tasks [51], with an end goal of integrating the fields of micromanipulation and microrobotics.

5. Trapping via integrated optics

Trapping nanoparticles, or submicrometer particles, in subdiffraction-limited regimes can be achieved by using optical near-fields. These can provide high electromagnetic field gradients near dielectric surfaces, opening up attractive avenues of research for optical trapping. Optical near-fields generally take the form of evanescent fields that decay exponentially from their point of origin. The first work that made use of the evanescent fields produced by a dielectric channel waveguide was published in 1996 by Kawata and Tani [52]. Here, the authors used only the evanescent field to propel latex particles of 5.1 μm in diameter along the length of a channeled waveguide at a speed of approximately 5 μm s^{-1} using only 80 mW of input laser power. While the particles propeled were of a relatively large size, it was the first work that highlighted the applicability of evanescent fields to particle trapping. Some of the following applications can be classified as tweezers, since they allow for full 3D confinement of the particle, while others only provide confinement in fewer dimensions.

5.1. Channel waveguides

Evanescent fields that extend beyond the boundary of light-carrying structures become more intense as the dimensions of the waveguide approach the wavelength of the guided light or become smaller [53]. This arises due to the wave nature of light that imposes certain boundary conditions on the structures in which they can exist. Evanescent fields play an indirect role in many plasmonic structures, primarily because they are used to excite SPPs via the Kretschmann configuration (see Section 6.1). However, there are many structures where the evanescent field can be accessed directly to trap particles. The evanescent field from a single beam propagating in an evanescent waveguide provides a gradient force that attracts particles towards the surface, while a simultaneous scattering force is applied in the direction of beam propagation. Hence, single-beam evanescent field traps are useful for guiding particles along the surface of a waveguide, making them ideal for integration with microfluidic systems.

An example of microfluidic/evanescent systems, is described in a paper by Schmidt et al. [54] where they demonstrated how particles could be trapped and propeled using channel waveguides in conjunction with microfluidic channels (Fig. 8). This work provided a clear and concise explanation of the physics at play in optofluidic systems, as well as displaying the trapping and propulsion of particles of varying size. Similarly, Yang and Erickson [55] have analyzed optofluidic particle trapping near waveguides. Building on these works, Ng et al. showed that gold colloidal particles as small as 17 nm could be propeled along a channel waveguide [56]. Using branched channel waveguides, or branched microfluidic channels, other groups have been able to extend these ideas to particle sorting [57, 58]. The attractiveness of these approaches comes from the fact that

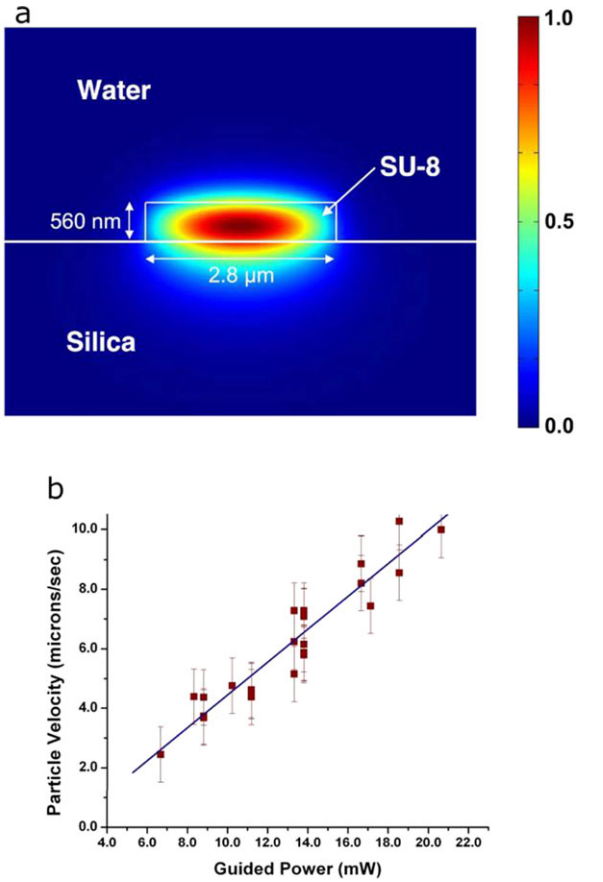

Figure 8 (a) E-field intensity plot of the channel waveguide. (b) Particle velocity versus guided power of a 3 μm particle trapped and propelled along a waveguide. (Reproduced with permission.[54] 2007, Opt. Express)

microfluidic channels and channel waveguides can be run parallel to each other, or even inside each other. Simple waveguides can also be arranged such that they produce resonating structures. Lin et al. [59] showed how microparticles can be trapped above a planar silicon microring resonator with large trapping depths of 25 k_bT.

There is a current trend in scientific research to encourage the development of "lab-on-a-chip" devices. Channel waveguides perfectly fit the requirements of a lab-on-a-chip device as they operate at the correct scale, can be mass produced, and are easily integrated with many existing technologies [60].

5.2. Optical micro- or nanofibers

Optical micro- or nanofibers (MNFs) are optical fibers with micrometer or submicrometer diameters that do not operate in the weakly guided regime. They are sometimes used to trap particles in their evanescent fields [61–64]. MNFs are, generally, manufactured from standard communication-grade optical fibers by heating them until they became malleable, at which point a force is applied from either

side to elongate and taper the heated region until the central (waist) region of the fiber is micrometer or submicrometer in diameter. A more detailed description of this heat-and-pull procedure can be found in the literature [65, 66]. In contrast, channel waveguides typically need to be grown on a substrate that, while allowing for complex geometries to be fabricated, somewhat limits their versatility. For example, some studies in neurobiology require a probe that can reach deep inside tissues in vivo. Very recently, optogenetics has come to the fore in neuroscience, and relies heavily on the use of optical fibers due to their ability to guide light into areas that are inaccessible using other methods [67]. While these techniques do not directly make use of the evanescent field or particle trapping, they emphasize the flexibility that is introduced once one moves from a platform consisting of rigid channel waveguide structures towards the use of tapered fibers. Fiber-based waveguides are capable of trapping and guiding particles as efficiently as their substrate-grown counterparts [62, 68, 69].

The use of a near-field scanning optical microscope to create a fiber optical tweezers (FOT) was realized by Xin et al. [70] and used to reliably trap micrometer-sized particles, but also showed that smaller particles such as yeast, bacteria, and 0.7-μm silica beads could be trapped, albeit with higher laser powers.

To realize a device whose operation is closer to that of optical tweezers, but with only the use of the evanescent fields produced by waveguides, one must consider counterpropagating laser beams [71–73]. Here, a standing wave can be formed that produces a potential landscape that favors the trapping of particles at certain lattice sites defined by the wavelength of light used. In practice, a standing wave is not entirely necessary for successfully immobilizing particles. Lei et al. [74] showed that, by varying the power of two counterpropagating beams, without the formation of a standing wave, particles with a diameter of 710 nm could be transported in either direction along a fiber. This was a useful study as it showed that standing waves are not necessary for the controlled guidance of micro- and nanoparticles along a tapered optical fiber.

Particle sorting using counterpropagating beams of different wavelengths relies on the scattering force's dependence on particle size, refractive index, and the wavelength of light used [75, 76]. Zhang and Li [75] used a subwavelength optical fiber with different wavelengths of light injected at either end (Fig. 9). The difference in scattering for various particle sizes resulted in the particles being sorted by size.

As is the case for optical tweezers, higher-order modes can be used to trap particles in waveguides. MNFs are an ideal platform for this, as they are capable of supporting many higher-order modes [77, 78], including Bessel-beams [79]. Higher-order mode trapping in straight, channel waveguides has been realized [80], but maintaining these modes in tapered fibers has proven to be a difficult process due to the fine degree of control required during the fabrication process, although it has been performed successfully using linearly tapered optical nanofibers [81]. Adiabaticity requirements impose important shape requirements on the taper profile and the dimensions of the fiber at the waist must also be considered. These combined conditions require a more complex tapering system [66] than is usually available to research groups. The use of higher-order modes in fibers for the purposes of atom trapping has been discussed elsewhere [82, 83].

5.3. Slot waveguides

When two waveguides are placed in close proximity to each other, as is the case in slot waveguides, the evanescent fields of the two waveguides overlap, producing a region of increased intensity between them [84]. Yang et al. have published a series of papers [85, 86] where polystyrene and gold particles are trapped in an optofluidic system consisting of a silicon slot waveguide grown on a glass substrate. The small waveguide separation, combined with the overlapping evanescent fields, provides a subdiffraction-limited trapping potential (Fig. 10). The authors were able to trap 75-nm dielectric nanoparticles and λ-DNA molecules using this waveguide system. Lin and Crozier [87] applied this technique to the problem of particle sorting. They used a channel waveguide that ran parallel to a slot waveguide. By introducing a defect, in this case a microsphere that had been fused to the channel waveguide, they were able to 'kick' smaller particles out of the potential formed by the channel waveguide and into the potential generated by the slot waveguide, which had a higher field confinement. Initially, 350-nm and 2-μm particles were guided along the channel waveguide. Upon reaching the defect, the 350-nm particles were pushed more than 250 nm away from the channel waveguide where they were then captured by the potential of the slot waveguide.

The use of evanescent devices to trap and manipulate micro- and nanoparticles continues to be of interest in the scientific community because of their versatility and customizability. Channel waveguide structures can be incorporated into almost any device at the fabrication stage and are produced using common industrial techniques. This makes their potential uses in commercial products more likely than other, more specialized, devices that are produced by nonscalable, multistage techniques.

5.4. Photonic crystal cavities

With the goal of confining light to subdiffraction-limited sizes, many research groups have focused their interest on photonic crystal (PC) cavities. Photonic crystal structures consist of a waveguide which has been periodically patterned to forbid the transmission of specific wavelengths. If, however, one introduces a defect to this periodic lattice it is possible to create a region where frequencies that were previously forbidden are now allowed to propagate. By choosing the defect carefully, a cavity can be set up within the crystal structure [88, 89]. If the wave vector of this new cavity mode is chosen so that it is also a confined mode of the waveguide, both lateral and inplane confinement is possible [90]. Photonic crystal cavities have some interesting

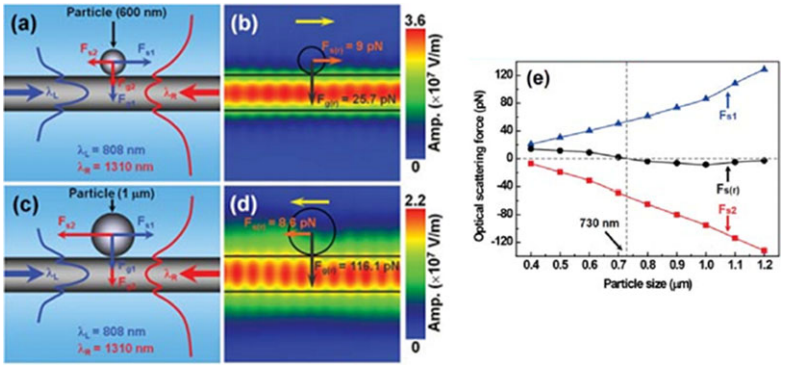

Figure 9 (a-d) Visualisation of the difference in the forces applied to 600 nm and 1000 nm diameter particles due to two different wavelengths counter-propagating along a tapered optical fibre. (b) and (d) are simulation results corresponding to (a) and (c) respectively. (e) A graph of the optical scattering forces on different particle sizes due to different wavelengths. Here, the blue line is the scattering from 808 nm light while the red line shows the scattering from the 1310 nm light, finally, the black line shows the contribution of both fields to the total scattering force acting on the particle. (Reproduced with permission.[75] 2013, Laser Photon. Rev.)

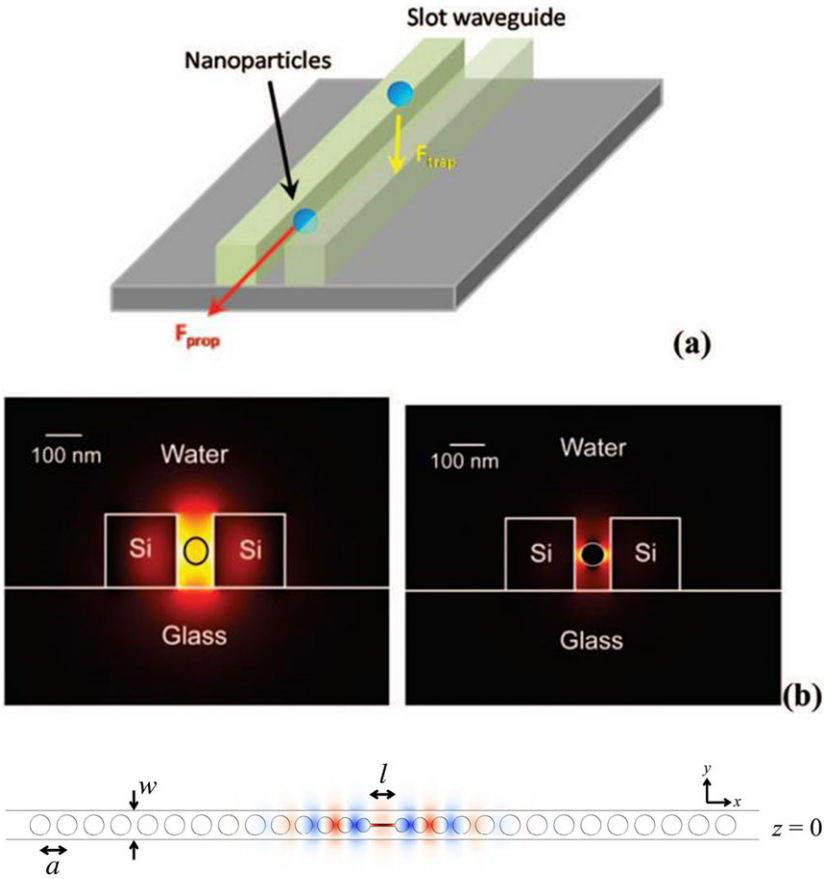

Figure 10 (a) Slot waveguide, (b) electric field intensity profiles for 65 nm polystyrene particles (left), and 100 nm gold particles (right). (Reproduced with permission.[85] 2009, Nano Lett.)

Figure 11 A typical linear photonic crystal cavity showing the field enhancement in the central slotted region. (Reproduced with permission.[90] 2013, Opt. Express)

properties that are advantageous for trapping particles. Robinson et al. [91] showed that the modes present in such structures have "ultrasmall" mode volumes. This leads to extremely high field gradients over subwavelength dimensions; the confinement of the electric field is comparable to the defect size used to create the cavity. A typical PC cavity is shown in Fig. 11.

Particle trapping using photonic crystal cavities was shown to be theoretically possible by Barth and Benson in 2006 [92]. They concluded that, not only could particles of varying sizes be trapped with a PC cavity, but the presence of the particles could shift the cavity resonance, a process known as self-induced back action (SIBA) which is discussed in more detail in Section 6.3. PC cavity devices have distinct advantages over other evanescent field-based devices. For example, Lin et al. [93] showed theoretically that, by tapering the angle of a PC cavity and including a slot, the gradient force could be significantly improved over that given by a waveguide alone, and that a high quality (Q) factor can be maintained.

By tapering a PC cavity, as shown in Fig. 12, an interesting method of controlling a particle's position was achieved [94]. The angle with which such a device is tapered controls the distance along the z-axis at which different wavelengths are reflected. This, in turn, produces trapping potentials at different locations depending on the

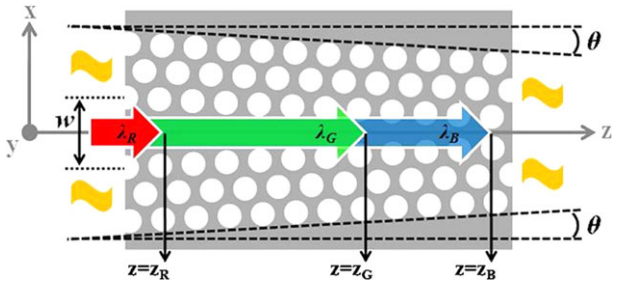

Figure 12 Tapered photonic crystal cavity. z_R, z_G, and z_B are the locations where light of three different colours — red, green, and blue — are reflected. (Reproduced with permission.[94] 2011, Opt. Lett.)

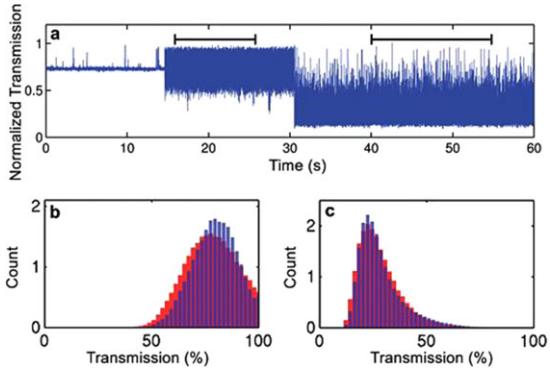

Figure 13 (a) Normalized transmission of the PC cavity system. (b) and (c) are histograms of the data highlighted with the horizontal bars at the left and right of (a) respectively. The histograms of the time series data (red) are given alongside the simulated histogram data (blue). Simulations were performed with a mean particle diameter of 24.8 nm (b) and 30 nm (c). (Reproduced with permission.[100] 2014, Nano Lett.)

frequency of the laser light. Using a tuneable laser source, particles can be moved along the axis of a PC cavity waveguide by gradually varying the wavelength and allowing the trapped particle to follow the changing trap position. Some uncertainity in the particle's position is introduced since the potentials created have multiple minima. However, input powers of 7 mW could, theoretically, trap 50-nm particles stably. PC cavities have also been integrated into optical fibers via femtosecond laser ablation processes, as well as composite systems comprising of MNFs in optical contact with external nanostructured gratings [95, 96]. PC cavities offer an effective way of trapping dielectric particles. Recently, van Leest and Caro [97] were able to stably trap single bacteria of two different species with an inplane trap stiffness of 7.6 pN nm^{-1} mW^{-1}.

Surface traps have also been formed using photonic crystal structures that do not rely on the introduction of a defect. For example, Jaquay et al. [98] used a photonic-crystal structure where the light was incident perpendicular to the apertures. This produced a lattice potential that caused particles to congregate and form large self-assembled arrays, a process that they referred to as light-assisted self-assembly (LATS) [99]. Work performed by Mirsadeghi and Young [100] using PC cavities have shown that they are a useful tool for trapping nanoscale particles and providing a means by which the size of the trapped particle can be determined with nm precision. By introducing a single-mode channel to a PC structure, particles as small as 24 nm were trapped. Analysis of the transmission spectra obtained over a number of trapping events was used to determine the mean diameter of the trapped particles by assuming some variance in the particles' polarizabilities, as shown in Fig. 13. As a particle trapping device, PC cavities are promising and their integration into existing technologies makes them an attractive choice for future progress in the trapping of particles.

5.5. Microlenses

Microlenses with diameters greater than the wavelength of light can also be used to trap particles in regular arrays. Zhao et al. [101] used arrays of 22 μm microlenses to trap 3.1-μm polymer particles. The relative ease of operation and reliability of such a macroscopic device makes it of interest for applications in the life sciences where high optical alignment may not be available. More recently, a similar device was made using femtosecond laser ablation [102].

6. Plasmonic-based devices

As particle sizes become smaller, problems associated with gradient force trapping arise. There are two options to enhance trapping at nanometer scales. One can choose to increase the power to further deepen the optical trap, but this is not usually viable as it is advisable to keep powers at a lower level to reduce noise and lessen power-induced damage to the trapped object. This means that one must increase the confinement of the laser light by some other means. Plasmonic structures have come to the fore in this regime.

The effect of surface plasmons on metallic nanostructures of varying designs is being actively pursued for particle trapping [7,103]. Nowadays, many research groups have access to a wide array of lithography techniques, allowing the creation of arbitrarily shaped designs. Furthermore, access to finite-element and FDTD software packages allow researchers to model how light interacts with plasmonic materials, photonic crystals, III-V semiconductors, etc., to a high degree of accuracy. With this arsenal of tools at hand, it is no surprise that the number of publications in the field has been rising rapidly in the last decade.

6.1. Surface plasmon polaritons and localized surface plasmons

Using plasmonic techniques, light can be concentrated to areas that are significantly below the diffraction limit.

Surface plasmons can be considered differently depending on the geometry of the substrate in question as either localized surface plasmons (LSPs), or as propagating surface plasmon polaritons. For brevity we will refer to the latter simply as surface plasmon polaritons (SPPs). Surface plasmons are the result of coherent electron oscillations on a metal's surface. SPPs are a means of quantifying how they behave on larger metallic surfaces that are capable of supporting propagating plasmon waves. SPPs cannot be directly excited with laser light since they exist as a wave propagating along the dielectric surface interface and their dispersion curves prohibit direct phase matching with an incident laser beam. Instead, they must be excited by an evanescent field. Currently, the most popular method of coupling to SPPs is called the Kretschmann configuration. This configuration makes use of total internal reflection through a glass prism. The required plasmonic structure need only be placed on one face of the prism, thus enabling it to be excited by the evanescent field generated by the reflection of the incident light passed through the prism at the critical angle. LSPs, on the other hand, define how surface plasmons behave on smaller surfaces where the boundary conditions cause confinement of the surface plasmon. LSPs are present in nanoparticles and wavelength-scale plasmonic geometries. Due to spatial confinement, phase matching is relaxed and, therefore, only light matching the correct LSP resonance frequency is required to excite them in a material. SPPs have a wide frequency range over which they can be excited, which is not the case for LSPs.

The form of an SPP is dictated largely by the geometry of the substrate and the input light field. That is not to say they are the only factors; of course, refractive indices and other material properties are important. A recent paper by Tsai et al. [44] showed how an SPP with a topological charge of 2, that is to say an SPP that contains orbital angular momentum, could be produced by using circularly polarized light in combination with a unique surface geometry. By etching an Archimedes spiral into a gold film, they were able to both confine a particle, and impart angular momentum to the particle, thereby causing it to rotate.

Heating due to inevitable ohmic losses in the metal is an intrinsic property of plasmonic devices, especially when devices based predominantly on the excitation of LSP modes are considered. The interaction between laser light and nanoparticles causes the generation of point-like heat sources at locations that depend on factors, such as particle type, beam polarization, and angle of incidence. Intense light fields generated near plasmonic nanostructures are often used to trap particles [104–106]. In some cases, the heat generated by the structures themselves was used to trap particles [107]. Because of this, analyzing heating effects is important. Donner et al. [108] discussed how the plasmon-assisted optofluidics is influenced by the heat produced. In short, this paper concluded that, for isolated nanostructures below 200 nm, the influence of heating is negligible. The authors also state that, to increase the plasmon-assisted fluid motion from tens of nanometers to hundreds of nanometers, structures larger than 1 μm must be used. Larger structures are easily integrated with heat sinks to help quickly dissipate the accumulated heat [109].

A recent study by Roxworthy et al. [110] on the heating effects of a 9×9 array of gold BNAs (bowtie nanoantenna apertures) in a SiO_2/ITO substrate has shown that heat-induced convection currents of greater that 1 μm s^{-1} can be created. The study gives both theoretical and experimental results that are quantitatively in agreement with each other. Seol et al. [111] showed that heating involved with the trapping of gold nanoparticles can also affect the spring constant of an optical trapping system. Because of this heating, they concluded that gold nanoparticles are not recommended when working with biological systems. Despite this, other authors have performed experiments with gold nanoparticles which seem to be in contradiction. For example, Demergis et al. showed ultrastrong binding of metallic nanoparticles via the optical binding force and estimated that there was no heating, contrary to other reported studies on similar systems [112].

6.2. Scalability

Surface plasmon polaritons on metallic surfaces sufficiently larger than the plasmon wavelength can be characterized as SPPs. Under these conditions, it can be assumed that the dispersion curve of the structure approaches that of an infinite metallic film [113]. This relationship is important as it shows that plasmonic-based devices cannot be scaled down ad infinitum. Devices that may work well at a few micrometers cannot be expected to work analogously at the nanometer scale. For example, in an experiment performed by Wong et al. [113], a dielectric channel optical waveguide was integrated with an array of gold micropads of 5 μm diameter and with a pitch of 15 μm. Figure 14 shows a schematic of the system. The authors trapped 5-μm polystyrene beads and yeast cells using an input beam power of 20 mW. This technique works well and relies on the formation of SPPs to create adequate trapping potentials above the discs. A similar paper by Righini et al. [114], where a prism was used to excite the SPPs, showed similar results. It should be obvious that simply downscaling the dimensions will not yield the same results. First, the plasmon will cease to be describable as a SPP once the pad size is reduced sufficiently in size, behaving instead as an LSP, and secondly, the viscous damping of suspended particles is greatly reduced due to the decreased cross section of smaller nanoparticles.

Gold nanopads were used by Chen et al. [115] to trap 500 nm and 100 nm nanoparticles using the LSPs generated in subwavelength disk structures. A seven by seven array of four gold circular nanopads was patterned on an indium titanium oxide substrate and illuminated by a Gaussian beam (Fig. 15). The nanopads were 200 nm in diameter, which produced polarization-dependent LSPs. This work was inspired by the earlier work in [41] and produced a similar washboard-type potential, thus drawing particles towards the center of the plasmonic structure.

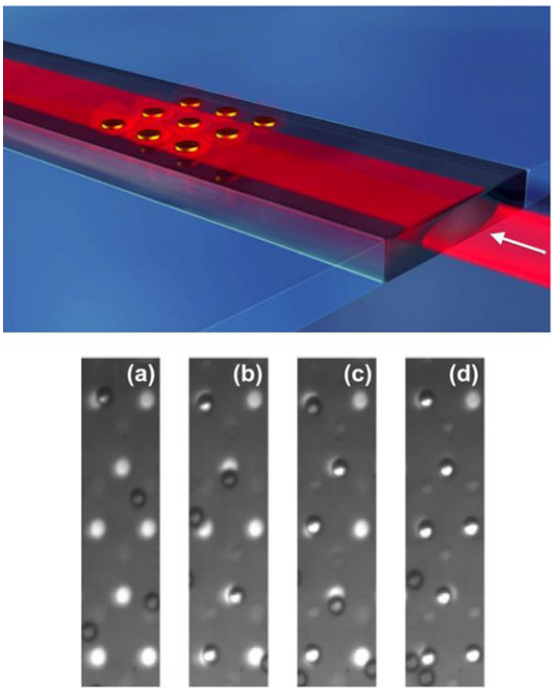

Figure 14 Channel waveguide incorporating a plasmonic gold micropad array. (a) – (d) are a time sequence of images showing the parallel trapping of 5 μm polystyrene beads. (Reproduced with permission.[113] 2011, Appl. Phys. Lett.)

6.3. Self-induced back action

Often, calculations on the trapping capabilities of optical tweezers are done in the absence of any particles. In many cases this is an appropriate choice, as it both simplifies the physics, from a computational viewpoint, and gives quantitatively accurate results. However, as particle sizes become smaller, and lower optical powers are used, it is necessary to include the effect of the dielectric particle on the local electric field, especially when plasmonic effects are present. The effect of a single particle tends to improve certain types of optical trapping via a mechanism called self-induced back action (SIBA). This effect has been studied in various systems, such as plasmonic and photonic crystal cavity systems, as mentioned earlier [116].

SIBA is especially relevant in many plasmonic structures as the effect plays a large role at the scales typically used. Juan et al. [116] trapped 50-nm nanoparticles using 2 mW of power with the help of SIBA. By cutting a 310-nm circular aperture into a 100-nm thick gold film a near-field was generated, which, in the presence of a dielectric particle, created a system that was sensitive to small position variations (Fig. 16). The particle present in the vicinity of the aperture effectively 'saw' a larger hole due to the shifting of the cutoff wavelength, thereby causing higher transmission of light through the aperture. Deviations of the particle from the equilibrium position near the aperture either increased or decreased the net transmission of light through the aperture. The authors showed that the particle's

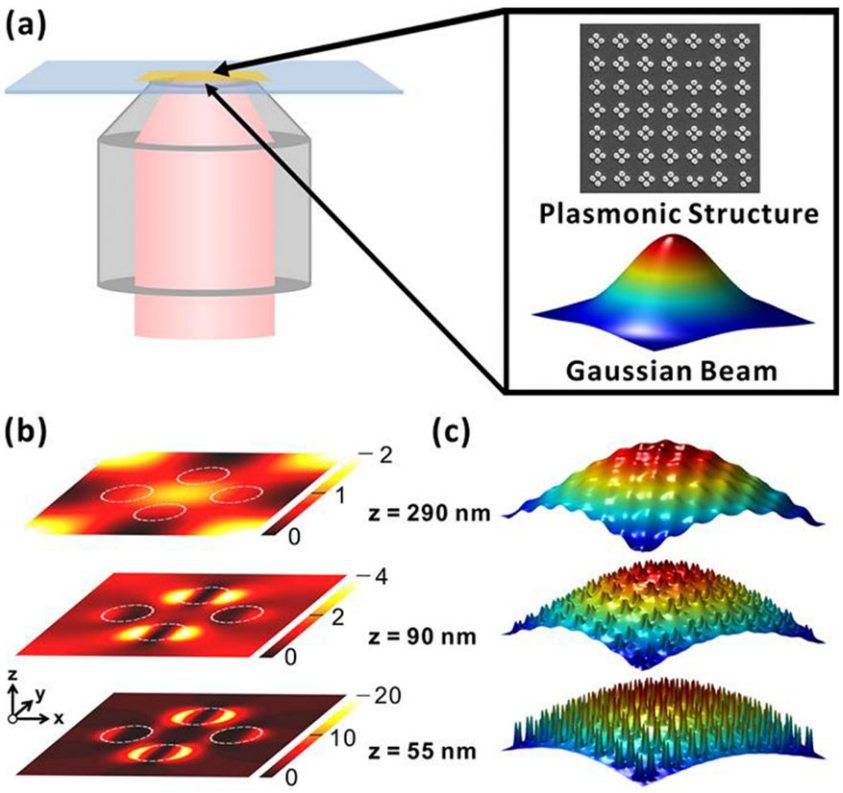

Figure 15 (a) Plasmonic disk array placed on an objective lens. (b) Light intensity at various heights above the disks. (c) Visualisation of the intensity profile at varying heights. (Reproduced with permission.[115] 2013, Nano Lett.)

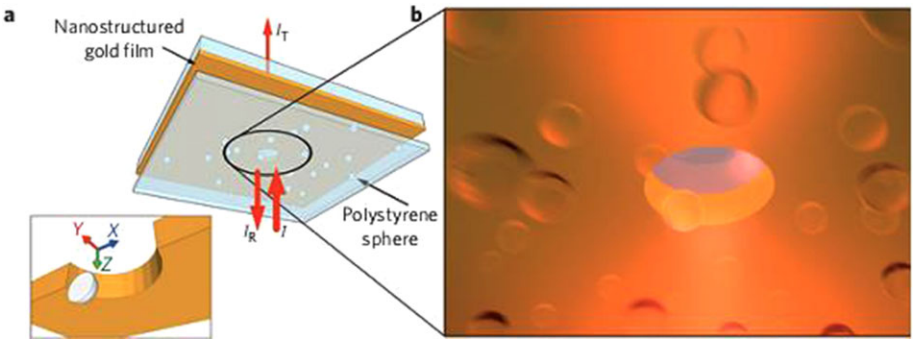

Figure 16 (a) An image showing the structure used to examine self-induced back action. (b) A closer view of the nanohole in the gold substrate. (Reproduced with permission.[116] 2009, Nat. Phys.)

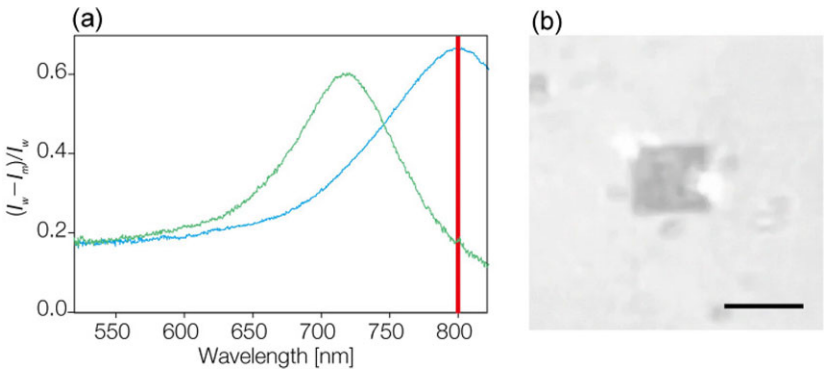

Figure 17 (a) Extinction spectra of a pair of gold nanoblocks with longitudinal (blue) and transverse (green) polarisations. (b) Plasmonic trapping of a 350 nm particle (bright region) using 80 nm $\times$ 80 nm $\times$ 40 nm nanoblocks as the polarisation is shifted between longitudinal and transverse. Scale bar $= 3\ \mu$m. (Reproduced with permission.[117] 2011, Opt. Express)

motion always served to create a force that pushed the particle back to its equilibrium position.

6.4. Superresolution optical trapping

Localized surface plasmons can be used for enhanced trapping well below the diffraction limit. Tanaka et al. referred to this ability as superresolution optical trapping [117]. Their plasmonic structure consisted of only two square gold nanoblocks, as shown in Fig. 17. This paper is indicative of this subfield of plasmonic trapping, in so much as how it highlights the importance of the choice of polarization in LSPs. Two important cases are considered, one parallel to the axis joining the two squares, and one at 90^o to this. The two cases highlight the fact that the device has various available modes and, by changing the polarization, specific modes can be excitied individually. The first configuration creates a single high-intensity spot between the two squares, whereas the latter allows for the creation of multiple trapping potentials with a subdiffraction-limit separation. Using gold nanoblocks the authors succeeded in trapping 100-nm polystyrene particles and observed double well potentials with 230 nm separation.

Gold bowtie nanoantenna apertures (BNAs) such as those created by Roxworthy and Toussaint [104] allow for trapping using LSPs (Fig. 18). They created an array of BNAs and, instead of using a standard continuous-wave (CW) laser source, they used a pulsed femtosecond (fs) laser source to trap dielectric and metallic particles. They observed increased trap stiffness over a CW approach while providing the ability to observe nonlinear effects in situ, such as two-photon absorption, second-harmonic generation, etc. The BNA arrays, however, coupled with the fs laser source, caused some of the spheres to adhere to the surface. The effect did not seem to be caused by the melting of the spheres, since the heat generated was not sufficient for this to occur. Rather, the induced heating seemed to attract particles to the BNA surfaces. The authors acknowledged that a theoretical model for optical tweezing using fs laser sources did not yet exist and did not attempt to explain the dynamics of the interaction in such a way. The increased trap stiffness was attributed to the illumination spot size of the laser source. Many BNAs were illuminated at once allowing particles to 'see' the effect of multiple traps, which, in turn, caused the particle's motion within the trap to be describable as acting with an effective trap stiffness with multiple contributions. Once again, fs laser sources are an interesting choice since they have the potential to reduce the overall power transferred to the trapped particles. In this experiment the power levels were three orders of magnitude lower than the optical damage threshold, as reported in [118].

Particles with a high polarizability are good for optical trapping, especially if a high refractive-index contrast between them and the surrounding material can be obtained. J-aggregrates, or Jelley aggregrates to give them their full name, were discovered independently by Scheibe et al. [119], and Jelley in 1937 [120]. J-aggregrates are essentially dye clusters with an absorption band that can be shifted. Zamecnik et al. [121] showed that by functionalizing these

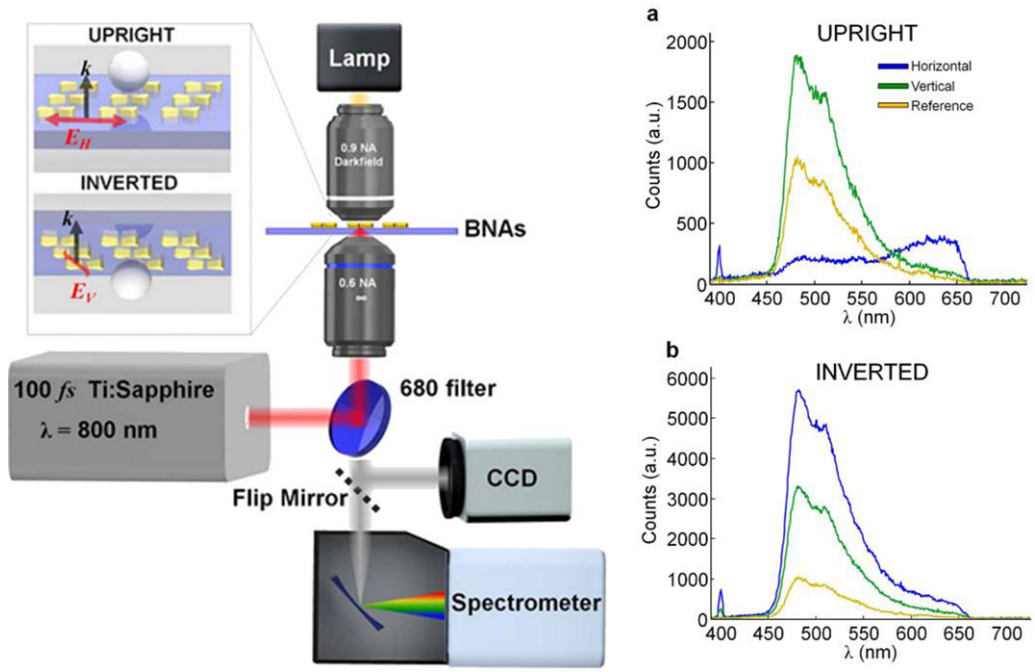

Figure 18 Au bowtie nanoantenna arrays in upright and inverted configuration and the associated experimental setup. Two-photon fluorescence measurements from a trapped fluorescent microsphere are given in (a) the upright orientation and (b) the inverted orientation. Blue and green curves represent the horizontally and vertically-polarized results, respectively. Yellow is a reference signal from a particle trapped on the glass substrate. (Reproduced with permission.[104] 2012, Scientific Reports)

aggregrates onto plasmonic silver nanoparticles interesting effects could be seen. The authors considered a particular type of material, known as ε near-zero materials (ENZ). This is a branch of materials that has an effective ε value near zero when illuminated at certain wavelengths, thereby significantly enhancing the scattering cross section. The permitivity of a medium, ε, is a measure of how much resistance a medium has to an external electric field, which leads to the electric displacement field encountered in Maxwell's equations. The authors targeted this property by combining silver plasmonic nanoparticles with J-aggregrates. By illuminating the particle near the plasmonic resonant wavelength, the electric field was confined within the J-aggregrate, creating a high field in a tightly confined area. The authors used this effect to perform surface-enchanced Raman spectroscopy. ENZ materials have some promising uses in the field of particle trapping.

6.5. Gratings

Gratings etched onto metallic surfaces allow coupling to SPPs since the additional grating vector of the system allows for mode matching of the SPP to the incident light. As we know, light fields can be combined to produce interesting electric-field configurations, and SPPs, being a form of electromagnetic radiation, behave the same. Genevet et al. [122] showed how placing diffraction gratings on a gold surface can generate a plasmonic bottle beam (Fig. 19). When two 2-dimensional planes with intersecting directions of propagation meet, what is known as a cosine Gaussian beam

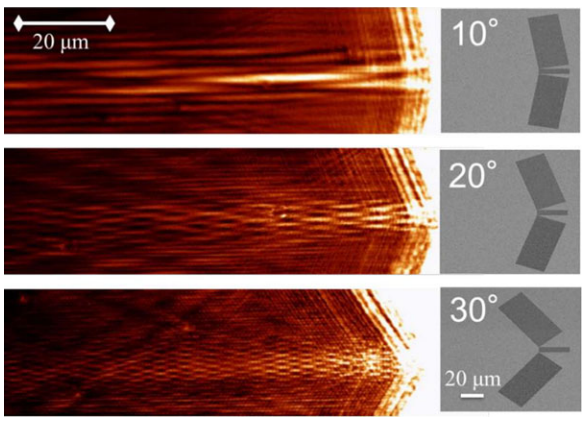

Figure 19 Near-field scanning optical microscopy images of plasmonic bottle beams generated at three different grating configurations. (Reproduced with permission.[122] 2013, Opt. Express)

(CGB) is formed. CGB are similar to Bessel beams since they have a nondiffracting nature in the direction of propagation. The authors applied this theory to SPPs. Using this property they were able to create an intensity profile that could trap particles at the nodes of high intensity.

6.6. Subwavelength apertures

Subwavelength aperture diffraction is, subject to debate, another area where plasmonics may play a role. Previously

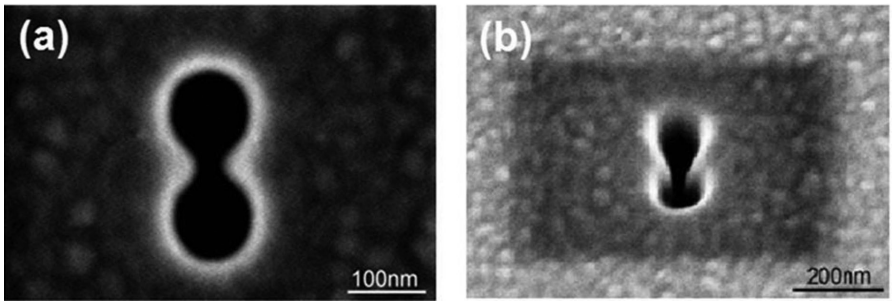

Figure 20 Double-nanohole created using a focussed ion beam in a gold layer. (Reproduced with permission.[126] 2012, Scientific Reports)

accepted theories, such as those by Bethe and Kirchoff, were used to model the propagation of light through apertures in either perfectly conducting screens, or black opaque screens. Given certain conditions these theories worked quite well, but did not provide an adequate explanation of how the light propagated through structures where the dimensions were below the cutoff for any mode to exist. A thorough review of previous and current theories on this type of diffraction is given by Weiner [123]. It was not until 1998 that a theory of plasmon assisted transmission through subwavelength apertures was proposed by Ebbesen et al. [124]. The authors showed that Bethe theory was wholly unsuitable to describe the transmission of light through subwavelength aperture arrays in a silver film. Surpisingly, they showed that transmission increased for wavelengths more than 10 times the diameter of the apertures and, in some cases, more light was transmitted than was directly incident on the apertures. These facts combined indicated that the apertures were more than just passive elements. The authors further showed that the behavior seemed to be independent of hole size and material type, yet had a strong angular dependence that could only be explained by the presence of surface plasmons. While plasmonics may play a role in the transmission through apertures, and for the case of gold materials they most certainly play some part, they are not entirely required to explain the dynamics of light transmission though Bethe apertures and this remains a point of controversy.

Baida and Van Labeke [125] performed work on annular aperture arrays that sought to increase the transmission of light via the same process as described by Ebbesen et al. [124]. Plasmonic double-nanoholes deal with the problem of transmission through subwavelength apertures. A typical double-nanohole is shown in Fig. 20. Using such a system, Zehtabi-Oskuie et al. [126] trapped 20-nm polysterene particles using as little as 3.5 mW of input power. A later analysis of the trapping efficiency was also produced by the same group [127], where they compared the trap stiffnesses obtained for a double-nanohole trap with that of a standard optical tweezers and claimed that similar trap stiffnesses can be obtained, but for particles that are 10 times smaller.

Building on the work by Baida and Van Labeke [125] many groups have pursued coaxial plasmonic waveguide structures for trapping [128–130]. Rodríguez-Fortuno et al. [128] predicted that coaxial plasmonic structures arranged in an array could be used as a negative refractive index material, a property that may be used to produce backwards travelling electromagnetic waves. Highly hybridized structures, such as the device proposed by Liu et al. [129], which combines gold annular aperture arrays with a photoresponsive liquid crystal, can also produce high field gradients in subdiffraction-limited regimes. All of these studies point towards a highly tuneable technique that has promising applications in particle trapping. Saleh and Dionne [131] published a theoretical paper where a gold coaxial plasmonic aperture in a silica fiber could be used to trap particles with sizes less than 10 nm. They also showed that the creation of dual trapping potentials at a distance of 20 nm from the surface is possible.

Subwavelength apertures in gold films can also be used in combination with tapered fibers. For instance, Neumann et al. [132] proposed the use of tapered optical fibers with subwavelength apertures to allow the high transmission of light to subdiffraction-limited spaces. The end face of a near-field scanning optical microscope (NSOM) probe was coated with gold and a focused ion beam was used to etch a 45-nm aperture into the gold layer. The NSOM taper was chosen such that it was near the cut-off diameter for the first excited mode, which was shown to be the case using numerical simulations. A more indepth discussion of the transmission mechanism has been published by Gordon [133]. He showed that transmission through the NSOM was improved by two orders of magnitude. Later, Berthelot et al. expanded on this idea by including a bowtie nanoaperture to the end face of a tapered optical fiber to allow three-dimensional manipulation of 50 nm dielectric objects (Fig. 21) [134]. The fields produced at the output of a half-tapered fiber, similar to an NSOM taper, are also capable of lensing light sufficiently to trap particles without any enhancements from plasmonic apertures.

7. Conclusion and outlook

In this review we have shown how the focus of particle trapping has recently been shifting from the micro- to the nanoscale by highlighting work in the field of optical manipulation, beginning with standard free-space beam-based optical tweezers and ending with more contemporary developments in the field of near-field optical trapping with special importance placed on those methods that circumvent the diffraction limit. It is clear that optical near-fields,

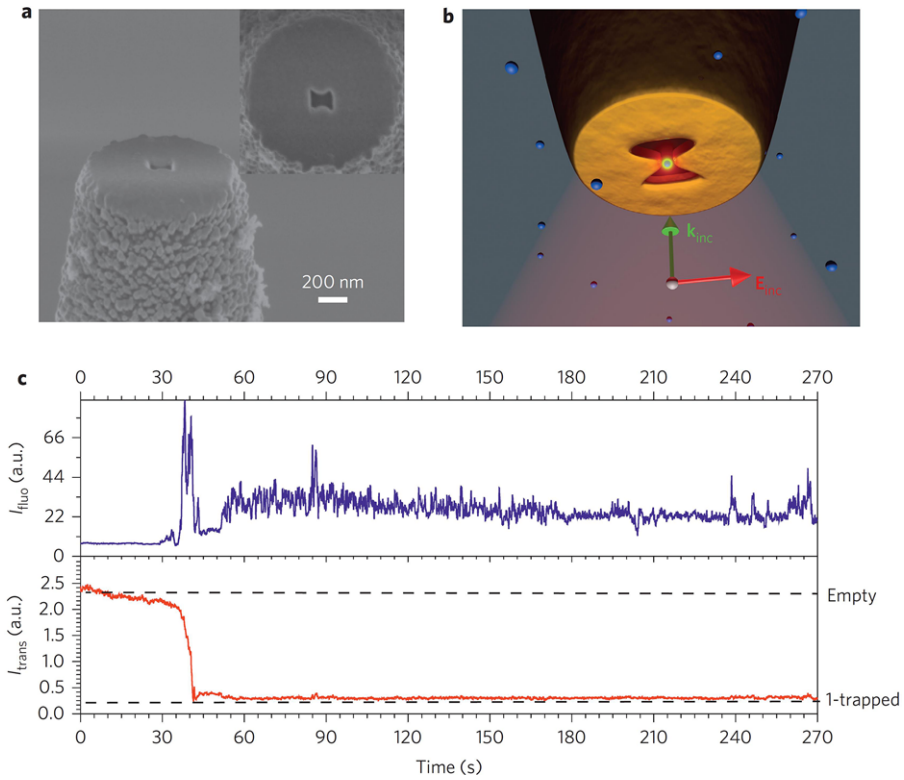

Figure 21 SEM image, (a), and schematic, (b), of an NSOM tip with a bowtie nanoantenna aperture located in the gold layer at the apex. (c) Time series of blue fluorescence from a dyedoped bead (blue line) along with the trapping beam intensity (red). A trapping event occurs at 40 s. (Reproduced with permission.[134] 2014, Nat. Nano)

in all of their forms, are the best solutions for overcoming this problem

Optical near-fields formed at dielectric-cladding interfaces in the form of evanescent fields present a potential path to nanoscale trapping, but, as has been shown, in order to generate the high confinement and required electric fields, simple waveguiding structures, such as ridge waveguides or MNFs, are insufficient. Enhancement of the fields, either through structural modifications, such as photonic crystal cavities, or the addition of plasmonic structures, is necessary to allow submicrometer trapping and manipulation.

The discovery of surface plasmons has arguably provided researchers with one of the most powerful tools to efficiently deal with the problem of trapping at the nanoscale. The low power requirements, high local field enhancements, and flexibility of design have been shown to provide many alternative methods for trapping nanoparticles. An end goal of this line of research is to provide life scientists with full 3D control over minute particles and further developments of the ideas and strategies presented in this paper may ultimately lead to devices that can operate well in the nanoscale regime. If a technique is developed that provides us with the ability to work in the nanoregime with the same degree of control as conventional optical tweezers provide in the microregime this will prove to be a huge boon to the scientific community at large.

Acknowledgements. This work was supported in part by funding from the Okinawa Institute of Science and Technology Graduate University. MS acknowledges the support of JSPS through the Postdoctoral Fellowship for Overseas Researchers scheme.

Received: 6 January 2015, **Revised:** 24 February 2015, **Accepted:** 12 March 2015

Published online: 15 April 2015

Key words: Optical trapping, optical tweezers, integrated optics, plasmonics.

References

[1] J. Kepler, De cometis libelli tres : I. Astronomicvs, theoremata continens de motu cometarum ubi demonstratio apparentiarum & altitudinis cometarum qui annis 1607. & 1618. conspecti sunt, ... : II. Physicvs, continens physiologiam comentarum nouam ... : III. Astrologicvs, de significationibus cometarum annorum 1607 and 1618 (typis Andreae Apergeri, sumptibus Sebastiani Mylii bibliopolæ augustani, Avgvstae Vindelicorum, 1619).
[2] J. H. Poynting, Nature **75**, 90 (1906).
[3] T. H. Maiman, Nature **187**, 493–494 (1960).
[4] A. Ashkin, J. M. Dziedzic, J. E. Bjorkholm, and S. Chu, Opt. Lett. **11**, 288–290 (1986).
[5] A. Ashkin, Phys. Rev. Lett. **24**, 156–159 (1970).
[6] J. B. Pendry, Phys. Rev. Lett. **85**, 3966–3969 (2000).
[7] M. L. Juan, M. Righini, and R. Quidant, Nature Photon. **5**, 349–356 (2011).
[8] R. Quidant and C. Girard, Laser Photon. Rev. **2**, 47–57 (2008).

[9] P. C. Ashok and K. Dholakia, Curr. Opin. Biotechnol. **23**, 16–21 (2012).
[10] F. M. Fazal and S. M. Block, Nature Photon. **5**, 318–321 (2011).
[11] M. P. Lee and M. J. Padgett, J. Microsc. **248**, 219–222 (2012).
[12] M. Waleed, S.-U. Hwang, J.-D. Kim, I. Shabbir, S.-M. Shin, and Y.-G. Lee, Biomed. Opt. Exp. **4**, 1533–1547 (2013).
[13] K. Svoboda, C. F. Schmidt, B. J. Schnapp, and S. M. Block, Nature **365**, 721–727 (1993).
[14] E. A. Abbondanzieri, W. J. Greenleaf, J. W. Shaevitz, R. Landick, and S. M. Block, Nature **438**, 460–465 (2005).
[15] N. Mortezaei, B. Singh, E. Bullitt, B. E. Uhlin, and M. Andersson, Sci. Rep. **3**, 3393 (2013).
[16] S. Lee and S. Hohng, J. Am. Chem. Soc. **135**, 18260–18263 (2013).
[17] I. Heller, G. Sitters, O. D. Broekmans, G. Farge, C. Menges, W. Wende, S. W. Hell, E. J. G. Peterman, and G. J. L. Wuite, Nature Meth. **10**, 910–916 (2013).
[18] R. Dasgupta, S. Ahlawat, R. S. Verma, and P. K. Gupta, Opt. Exp. **19**, 7680–7688 (2011).
[19] D. V. Petrov, J. Opt. A: Pure Appl. Opt. **9**, S139 (2007).
[20] I. Amato, Cell **123**, 967–970 (2005).
[21] H. Maruyama, K. Kotani, A. Honda, T. Takahata, and F. Arai, presented at the 10th IEEE Conference on Nanotechnology (IEEE-NANO), 2010 (unpublished).
[22] A. Ashkin, Phys. Rev. Lett. **40**, 729–732 (1978).
[23] S. Albaladejo, M. I. Marqués, M. Laroche, and J. J. Sáenz, Phys. Rev. Lett. **102**, 113602 (2009).
[24] H. C. van de Hulst, Quart. J. Roy. Meteorolog. Soc. **84**, 198–199 (1958).
[25] K.-N. Liou, Appl. Math. Comput. **3**, 331–358 (1977).
[26] A. B. Stilgoe, T. A. Nieminen, G. Knöner, N. R. Heckenberg, and H. Rubinsztein-Dunlop, Opt. Exp. **16**, 15039–15051 (2008).
[27] G. P. Krishnan and D. T. Leighton, Phys. Fluids **7**, 2538–2545 (1995).
[28] A. J. Goldman, R. G. Cox, and H. Brenner, Chem. Eng. Sci. **22**, 637–651 (1967).
[29] K. Visscher, G.J. Brakenhoff, and J. J. Krol, Cytometry **14**, 105–114 (1993).
[30] M. Padgett and R. Di Leonardo, Lab Chip **11**, 1196–1205 (2011).
[31] R. W. Bowman, G. M. Gibson, A. Linnenberger, D. B. Phillips, J. A. Grieve, D. M. Carberry, S. Serati, M. J. Miles, and M. J. Padgett, Comput. Phys. Commun. **185**, 268–273 (2014).
[32] B. Agate, C. Brown, W. Sibbett, and K. Dholakia, Opt. Exp. **12**, 3011–3017 (2004).
[33] K. Svoboda and S. M. Block, Annu. Rev. Biophys. Biomol. Struct. **23**, 247–285 (1994).
[34] Y. Deng, J. Bechhoefer, and N. R. Forde, J. Opt. A: Pure Appl. Opt. **9**, S256–S263 (2007).
[35] B. Lukić, S. Jeney, C. Tischer, A. J. Kulik, L. Forró, and E. L. Florin, Phys. Rev. Lett. **95**, 160601 (2005).
[36] K. Berg-Sørensen and H. Flyvbjerg, Rev. Sci. Instrum. **75**, 594–612 (2004).
[37] A. Balijepalli, J. J. Gorman, S. K. Gupta, and T. W. LeBrun, Nano Lett. **12**, 2347–2351 (2012).
[38] J. R. Moffitt, Y. R. Chemla, D. Izhaky, and C. Bustamante, Proc. Natl. Acad. Sci. **103**, 9006–9011 (2006).
[39] H. Sahoo, J. Photoch. Photobio. C **12**, 20–30 (2011).
[40] M. Woerdemann, C. Alpmann, M. Esseling, and C. Denz, Laser Photon. Rev. **7**, 839–854 (2013).
[41] S. A. Tatarkova, W. Sibbett, and K. Dholakia, Phys. Rev. Lett. **91**, 038101 (2003).
[42] M. Padgett and R. Bowman, Nature Photon. **5**, 343–348 (2011).
[43] L. Allen, M. W. Beijersbergen, R. J. C. Spreeuw, and J. P. Woerdman, Phys. Rev. A **45**, 8185–8189 (1992).
[44] W.-Y. Tsai, J.-S. Huang, and C.-B. Huang, Nano Lett. **14**, 547–552 (2014).
[45] T. Cizmar, V. Garcés-Chávez, K. Dholakia, and P. Zemanek, Appl. Phys. Lett. **86** 174101 (2005).
[46] G. Carmon and M. Feingold, Opt. Lett. **36**, 40–42 (2011).
[47] F. Borghese, P. Denti, R. Saija, M. A. Iatì, and O. M. Maragò, Phys. Rev. Lett. **100**, 163903 (2008).
[48] A. La Porta and M. D. Wang, Phys. Rev. Lett. **92**, 190801 (2004).
[49] S. H. Simpson, D. C. Benito, and S. Hanna, Phys. Rev. A **76**, 043408 (2007).
[50] T. Asavei, T. A. Nieminen, V. L. Y. Loke, A. B. Stilgoe, R. Bowman, D. Preece, M. J. Padgett, N. R. Heckenberg, and H. Rubinsztein-Dunlop, New J. Phys. **15**, 063016 (2013).
[51] D. Palima and J. Glückstad, Laser Photon. Rev. **7**, 478–494 (2013).
[52] S. Kawata and T. Tani, Opt. Lett. **21**, 1768–1770 (1996).
[53] A. W. Snyder and J. Love, Optical Waveguide Theory (Springer, 1983).
[54] B. S. Schmidt, A. H. Yang, D. Erickson, and M. Lipson, Opt. Exp. **15**, 14322–14334 (2007).
[55] A. H. J. Yang and D. Erickson, Nanotechnology **19**, 045704 (2008).
[56] L. N. Ng, B. J. Luff, M. N. Zervas, and J. S. Wilkinson, Opt. Commun. **208**, 117–124 (2002).
[57] K. Grujic, O. G. Hellesø, J. P. Hole, and J. S. Wilkinson, Opt. Exp. **13**, 1–7 (2005).
[58] R. F. Marchington, M. Mazilu, S. Kuriakose, V. Garcés-Chávez, P. J. Reece, T. F. Krauss, M. Gu, and K. Dholakia, Opt. Exp. **16**, 3712–3726 (2008).
[59] S. Lin, E. Schonbrun, and K. Crozier, Nano Lett. **10**, 2408–2411 (2010).
[60] D. Erickson, X. Serey, Y. F. Chen, and S. Mandal, Lab Chip **11**, 995–1009 (2011).
[61] F.-W. Sheu and Y.-S. Huang, Sensors **13**, 2884–2894 (2013).
[62] C. Xu, H. Lei, Y. Zhang, and B. Li, Opt. Exp. **20**, 1930–1938 (2012).
[63] A. Goban, K. S. Choi, D. J. Alton, D. Ding, C. Lacroûte, M. Pototschnig, T. Thiele, N. P. Stern, and H. J. Kimble, Phys. Rev. Lett. **109**, 033603 (2012).
[64] M. Morrissey, K. Deasy, M. Frawley, R. Kumar, E. Prel, L. Russell, V. Truong, and S. Nic Chormaic, Sensors **13**, 10449–10481 (2013).
[65] T. A. Birks and Y. W. Li, J. Lightwave Technol. **10**, 432 (1992).
[66] J. M. Ward, V. H. Le, A. Maimaiti, and S. Nic Chormaic, Rev. Sci. Instrum. **85**, 111501 (2014).
[67] E. Pastrana, Nature Meth. **8**, 24–25 (2011).

[68] G. Brambilla, G. S. Murugan, J. S. Wilkinson, and D. J. Richardson, Opt. Lett. **32**, 3041–3043 (2007).
[69] S. E. Skelton, M. Sergides, R. Patel, E. Karczewska, O. M. Maragó, and P. H. Jones, J. Quant. Spectrosc. Radiat. Transfer **113**, 2512–2520 (2012).
[70] H. Xin, R. Xu, and B. Li, Sci. Rep. **2**, 818 (2012).
[71] C. D. Mellor and C. D. Bain, Chem. Phys. Chem. **7**, 329–332 (2006).
[72] J. Lekner, J. Phys. B: At. Molec. Opt. Phys. **38**, 3849 (2005).
[73] K. Grujic and O. G. Hellesø, Opt. Exp. **15**, 6470–6477 (2007).
[74] H. Lei, C. Xu, Y. Zhang, and B. Li, Nanoscale **4**, 6707–6709 (2012).
[75] Y. Zhang and B. Li, Laser Photon. Rev. **7**, 289–296 (2013).
[76] M. Ploschner, T. Čižmár, M. Mazilu, A. Di Falco, and K. Dholakia, Nano Lett. **12**, 1923–1927 (2012).
[77] A. Petcu-Colan, M. Frawley, and S. Nic Chormaic, J. Nonlinear Opt. Phys. Mater. **20**, 293–307 (2011).
[78] M. Frawley, A. Petcu-Colan, V. G. Truong, and S. Nic Chormaic, Opt. Commun. **285**, 4648 (2012).
[79] T. Cizmar, V. Garcés-Chávez, K. Dholakia, and P. Zemanek, presented at the Proceedings of SPIE Vol. 5514, (2004) (unpublished).
[80] T. Tanaka and S. Yamamoto, Appl. Phys. Lett. **77**, 3131–3133 (2000).
[81] A. Maimaiti, V. G. Truong, M. Sergides, I. Gusachenko, and S. Nic Chormaic, Sci. Rep. **5**, 9077 (2015).
[82] J. Fu, X. Yin, N. Li, and L. Tong, Chin. Opt. Lett. **6**, 112–115 2008.
[83] R. Kumar, V. Gokhroo, K. Deasy, A. Maimaiti, C. Phelan, M. Frawley, and S. Nic Chormaic, New J. Phys. **17**, 013026 (2015).
[84] P. A. Anderson, B. S. Schmidt, and M. Lipson, Opt. Exp. **14**, 9197–9202 (2006).
[85] A. H. J. Yang, T. Lerdsuchatawanich, and D. Erickson, Nano Lett. **9**, 1182–1188 (2009).
[86] A. H. J. Yang, S. D. Moore, B. S. Schmidt, M. Klug, M. Lipson, and D. Erickson, Nature **457**, 71–75 (2009).
[87] S. Lin and K. B. Crozier, Opt. Exp. **20**, 3367–3374 (2012).
[88] B.-S. Song, S. Noda, T. Asano, and Y. Akahane, Nature Mater. **4**, 207–210 (2005).
[89] C. A. Mejia, N. Huang, and M. L. Povinelli, Opt. Lett. **37**, 3690–3692 (2012).
[90] P. Seidler, K. Lister, U. Drechsler, J. Hofrichter, and T. Stöferle, Opt. Exp. **21**, 32468–32483 (2013).
[91] J. T. Robinson, C. Manolatou, L. Chen, and M. Lipson, Phys. Rev. Lett. **95**, 143901 (2005).
[92] M. Barth and O. Benson, Appl. Phys. Lett. **89**, 253114 (2006).
[93] S. Lin, J. Hu, L. Kimerling, and K. Crozier, Opt. Lett. **34**, 3451–3453 (2009).
[94] P.-T. Lin and P.-T. Lee, Opt. Lett. **36**, 424–426 (2011).
[95] K. P. Nayak, P. Zhang, and K. Hakuta, Opt. Lett. **39**, 232–235 (2014).
[96] R. Yalla, M. Sadgrove, K. P. Nayak, and K. Hakuta, Phys. Rev. Lett. **113**, 143601 (2014).
[97] T. van Leest and J. Caro, Lab Chip **13**, 4358–4365 (2013).
[98] E. Jaquay, L. J. Martínez, C. A. Mejia, and M. L. Povinelli, Nano Lett. **13**, 2290–2294 (2013).
[99] C. A. Mejia, A. Dutt, and M. L. Povinelli, Opt. Exp. **19**, 11422–11428 (2011).
[100] S. H. Mirsadeghi and J. F. Young, Nano Lett. **14**, 5004–5009 (2014).
[101] X. Zhao, Y. Sun, J. Bu, S. Zhu, and X. C. Yuan, Appl. Opt. **50**, 318–322 (2011).
[102] J. Yong, F. Chen, Q. Yang, G. Du, H. Bian, D. Zhang, J. Si, F. Yun, and X. Hou, ACS Appl. Mater. Interfaces **5**, 9382–9385 (2013).
[103] R. Quidant, MRS Bull. **37**, 739–744 (2012).
[104] B. J. Roxworthy and K. C. Toussaint, Jr., Sci. Rep. **2**, 660 (2012).
[105] W. Zhang, L. Huang, C. Santschi, and O. J. F. Martin, Nano Lett. **10**, 1006–1011 (2010).
[106] M. Ploschner, M. Mazilu, T. F. Krauss, and K. Dholakia, J. Nanophoton. **4**, 041570 (2010).
[107] C. M. Galloway, M. P. Kreuzer, S. S. Aćimović, G. Volpe, M. Correia, S. B. Petersen, M. T. Neves-Petersen, and R. Quidant, Nano Lett. **13**, 4299–4304 (2013).
[108] J. S. Donner, G. Baffou, D. McCloskey, and R. Quidant, ACS Nano **5**, 5457–5462 (2011).
[109] K. Wang, E. Schonbrun, P. Steinvurzel, and K. B. Crozier, Nature Commun. **2**, 469 (2011).
[110] B. J. Roxworthy, A. M. Bhuiya, S. P. Vanka, and K. C. Toussaint Jr., Nature Commun. **5**, 1713 (2014).
[111] Y. Seol, A. E. Carpenter, and T. T. Perkins, Opt. Lett. **31**, 2429–2431 (2006).
[112] V. Demergis and E.-F. Florin, Nano Lett. **12**, 5756–5760 (2012).
[113] H. M. K. Wong, M. Righini, J. C. Gates, P. G. R. Smith, V. Pruneri, and R. Quidant, Appl. Phys. Lett. **99**, 061107 (2011).
[114] M. Righini, G. Volpe, C. Girard, D. Petrov, and R. Quidant, Phys. Rev. Lett. **100**, 186804 (2008).
[115] K. Y. Chen, A. T. Lee, C. C. Hung, J. S. Huang, and Y. T. Yang, Nano Lett. **13**, 4118–4122 (2013).
[116] M. L. Juan, R. Gordon, Y. Pang, F. Eftekhari, and R. Quidant, Nature Phys. **5**, 915–919 (2009).
[117] Y. Tanaka, and K. Sasaki, Opt. Exp. **19**, 17462–17468 (2011).
[118] M. Righini, P. Ghenuche, S. Cherukulappurath, V. Myroshnychenko, F. J. García de Abajo, and R. Quidant, Nano Lett. **9**, 3387–3391 (2009).
[119] G. Scheibe, L. Kandler, and H. Ecker, Naturwissenschaften **25**, 75–75 (1937).
[120] E. E. Jelley, Nature **139**, 631–632 (1937).
[121] C. R. Zamecnik, A. Ahmed, C. M. Walters, R. Gordon, and G. C. Walker, J. Phys. Chem. C **117**, 1879–1886 (2013).
[122] P. Genevet, J. Dellinger, R. Blanchard, A. She, M. Petit, B. Cluzel, M. A. Kats, F. de Fornel, and F. Capasso, Opt. Exp. **21**, 10295–10300 (2013).
[123] J. Weiner, Rep. Prog. Phys. **72**, 064401 (2009).
[124] T. W. Ebbesen, H. J. Lezec, H. F. Ghaemi, T. Thio, and P. A. Wolff, Nature **391**, 667–669 (1998).
[125] F. I. Baida and D. Van Labeke, Phys. Rev. B: Condens. Matter **67**, 155314 (2003).

[126] A. Zehtabi-Oskuie, J. G. Bergeron, and R. Gordon, Sci. Rep. **2**, 966 (2012).
[127] A. Kotnala and R. Gordon, Nano Lett. **14**, 853–856 (2014).
[128] F. J. Rodríguez-Fortuño, C. García-Meca, R. Ortuño, J. Martí, and A. Martínez, Opt. Lett. **34**, 3325–3327 (2009).
[129] Y. J. Liu, G. Y. Si, E. S. P. Leong, N. Xiang, A. J. Danner, and J. H. Teng, Adv. Mater. **24**, OP131–OP135 (2012).
[130] R. de Waele, S. P. Burgos, A. Polman, and H. A. Atwater, Nano Lett. **9**, 2832–2837 (2009).
[131] A. A. E. Saleh and J. A. Dionne, Nano Lett. **12**, 5581–5586 (2012).
[132] L. Neumann, Y. Pang, A. Houyou, M. L. Juan, R. Gordon, and N. F. van Hulst, Nano Lett. **11**, 355–360 (2010).
[133] R. Gordon, Phys. Rev. A **76**, 053806 (2007).
[134] J. Berthelot, S. S. Acimovic, M. L. Juan, M. P. Kreuzer, J. Renger, and R. Quidant, Nature Nano **9**, 295–299 (2014).